Significant Achievements in

Space Applications 1965

NATIONAL AERONAUTICS AND SPACE ADMINISTRATION

Significant Achievements in

⁊ Space
Applications
1965

Foreword

THIS VOLUME IS ONE OF A SERIES which summarizes the achievements made in the scientific and technical disciplines involved in the Space Science and Applications Program of the United States. The contribution made by the National Aeronautics and Space Administration is highlighted against the background of the overall progress in these disciplines. Succeeding issues will document the results from later years.

The achievements during the period 1958 to 1964 in the following areas were reported in NASA Special Publications 91 to 100: Astronomy, Bioscience, Communications and Navigation, Geodesy, Ionospheres and Radio Physics, Meteorology, Particles and Fields, Planetary Atmospheres, Planetology, and Solar Physics.

This volume summarizes the progress in space applications in 1965 in the following areas: Communications, Geodesy, and Meteorology. A companion volume (NASA SP—136) describes the significant scientific progress in 1965 in the following areas: Astronomy, Ionospheres and Radio Physics, Particles and Fields, Planetary Atmospheres, Planetology, and Solar Physics.

Although we do not here attempt to name all those who have contributed to the NASA program during 1965, both in the experimental and theoretical research, and in the analysis, compilation, and reporting of these results, nevertheless we wish to acknowledge all the contributions to a very fruitful program in which this country may take justifiable pride.

HOMER E. NEWELL
Associate Administator for
Space Science and Applications, NASA

iii

Preface

IN THE AREA OF SPACE APPLICATIONS, which may be defined as the practical exploitation of space technology to meet the needs of man and his society, we attempt to make use of space technology of general applicability, such as power systems, launch vehicle systems, structure and thermal control systems, and the like. We combine this capability with the unique instrumentation which is necessary to provide a better means of meeting practical needs of mankind in order to achieve communication over great distances, observation of weather patterns over great areas, and development of a precise knowledge of the detailed shape of the Earth to permit an accurate relative positioning of the continents.

Although there were no startling breakthroughs in 1965, the year was characterized by an orderly transition in our space program from the experimental toward the utilitarian in space applications.

The year 1965 marked the inauguration of a commercial, 24-hour, trans-Atlantic communications link capable of carrying not only voice and teletype data, thus supplementing undersea cables, but also television material. Its only competitor, the airplane, inserts hours of delay between the original transmission—transportation of the filmed or taped material—and the retransmission and reception of the recorded television program.

The final elements of technology necessary to commit meteorological satellites to an operational system were proved with the placement of Tiros IX and X in nearly polar Sun-synchronous orbits which permitted, for the first time, full coverage of the sunlit half of the globe throughout each day.

In the area of geodesy, two satellites were launched to develop further the instrumentation and techniques necessary to locate a satellite precisely in space and thus, by backtracking, to locate the observing stations with the same precision.

Many details of progress in space applications during 1965 are given in this volume; however, two points are of particular interest. First, a careful analysis of certain of the optical and infrared observations of the Earth from our meteorological satellites revealed that these data could provide information which falls in disciplines other than me-

teorology, such as oceanography, geology, and perhaps forestry. This finding encourages us to broaden our studies of the Earth from space with the expectation of practical, immediate, and direct benefit to man. Second, perhaps in reaction to the successful exploitation of communications satellites by the United States, initially in experimental roles and later in commercial intercontinental traffic, the U.S.S.R. in 1965 launched two experimental communication satellites and, after an experimental period, announced that they were being used, at least intermittently, for commercial service between Moscow and Vladivostok.

Contents

SATELLITE COMMUNICATIONS AND NAVIGATION

Donald P. Rogers

Space Applications Programs
Office of Space Science and Applications, NASA

Satellite Communications and Navigation

INTRODUCTION

As 1965 OPENED, the United States had five working active communications satellites and two passive communications satellites in orbit: Echo I and II, Telstar II, Relay I and II, and Syncom II and III. During 1965 there were no launches of experimental communications satellites; however, the first operational commercial communications satellite, Early Bird I, was launched on April 6, 1965, and was placed into commercial service across the Atlantic Ocean on June 28, 1965. At the close of 1965, four of the five experimental and the one commercial communications satellites were still working. Four of the seven experimental communications satellites had exceeded their design lifetime.

Echo I and II

Echo I and II remained in orbit throughout 1965 and, while communications experiments with these satellites were minimal, their orbital behavior was actively studied to evaluate the perturbing effects of varying air drag and solar activity. In addition, the two Echo satellites were reportedly used as passive geodetic satellites by many groups throughout the world, including those in countries behind the Iron Curtain.

Telstar II

Telstar II functioned satisfactorily throughout the year, although seldom observed since the conversion of the American Telephone & Telegraph Co. ground station at Andover, Maine, to commercial operations with Early Bird.

Relay I and II

Relay I ceased operating on February 11, 1965, after 26 months of useful life. Relay II continues to function satisfactorily. Since September 30, 1965, when the station at Mojave, Calif., was taken out of service, there have been no Relay communications experiments involving U.S. ground stations; foreign ground stations continued to utilize

3

Relay II, however. Data were taken routinely on an augmented schedule from the environmental experiments on Relay II.

Syncom II and III

Syncom II and III were transferred to the Department of Defense on April 1, 1965, and for the balance of the year they were used daily for communications in the Indian Ocean and Pacific Ocean areas. Figure 1 shows the locations of Syncom II and III.

In February 1965 Syncom II exhausted its propellant near an Earth-stable point (at 73° east longitude). As a consequence, its position over the Earth oscillates about the 73d east meridian yearly, from 65° east to 81° east, while continuing its daily figure-8 ground track, between 33° north and 33° south latitudes.
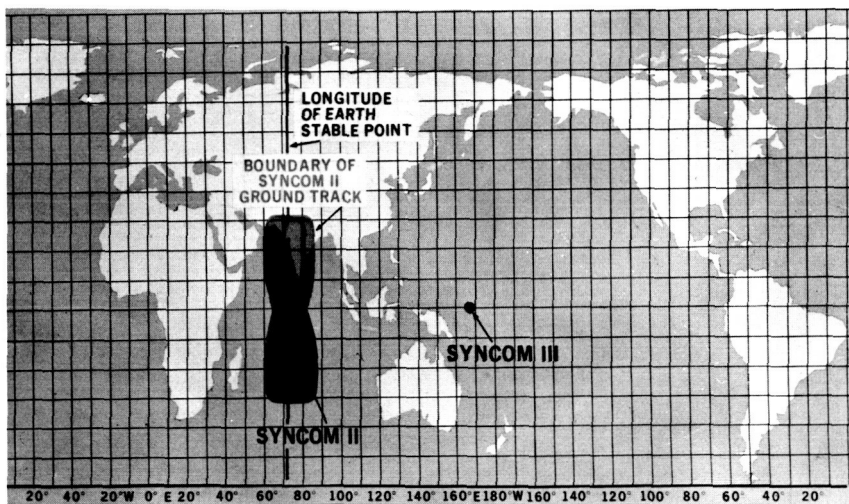
Figure 1.—Syncom II and III positions (December 1965).

Syncom III, the first geostationary satellite, was located above the Equator in the Pacific near 168° east longitude. At the end of 1965 its propellant supply was sufficient to maintain this location for an additional year.

COMMUNICATIONS SATELLITE CORP.

On April 6, 1965, the National Aeronautics and Space Administration launched the Early Bird satellite, shown in figure 2, for the Communications Satellite Corp., using a thrust-augmented Delta launch vehicle. The launch was carried out under the terms of an agreement between
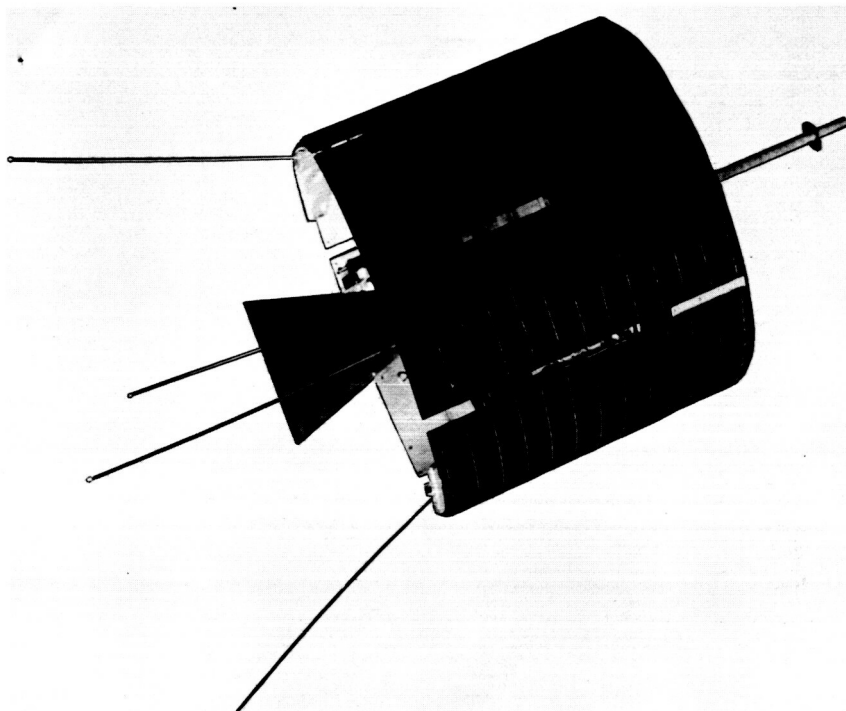
Figure 2.—HSHS–303 (Early Bird) satellite.

NASA and the Communications Satellite Corp., made in December 1964. According to this agreement, NASA would procure and test the launch vehicle, procure the apogee-kick motor, manage the integration of launch vehicle and spacecraft, carry out the launch, and provide certain postlaunch tracking and communications services.

In June 1965 the Communications Satellite Corp. was invited to propose to the Government a satellite system which could be used to provide operational support of the Apollo program. This proposal was received in August 1965 and accepted in October. The Corporation proposed a satellite larger and heavier than Early Bird (as shown in fig. 3) which would require a thrust-augmented improved Delta launch vehicle.

The Corporation also completed design studies of three types of satellites for a full-scale global system in February 1965. As a result of these studies, the Corporation decided in May to eliminate further consideration of satellites in random orbits and to continue with the design of a satellite capable of being used in either a phased medium-
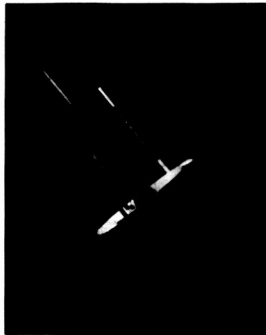
Early Bird
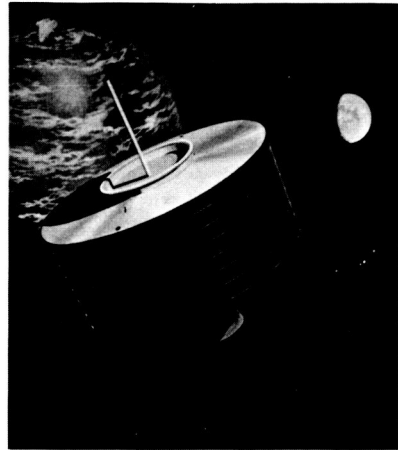
HS-303A

Figure 3.—Relative sizes of Early Bird and HS–303A.

altitude system or a synchronous system. Specifications for such a satellite were approved on August 11, 1965, and one contract was initiated for detailed satellite design.

FOREIGN COMMUNICATIONS SATELLITE ACTIVITY

Perhaps in reaction to the continuing success of the U.S. program in first-generation experimental communications satellites (which culminated in the formation of the Communications Satellite Corp. and the inauguration of commercial transatlantic service via Early Bird), the U.S.S.R. launched two experimental communications satellites during 1965: Molniya I–1 on April 23, 1965, and Molniya I–2 on October 14, 1965. These very large and heavy satellites were then placed in high, elliptical, 12-hour orbits with an apogee of almost 40 000 kilometers, a perigee of about 420 kilometers, and an inclination of just over 65°. This unique orbit has certain decided advantages for communications usage in the northern latitudes. The satellites reportedly have been used both for communications experiments and for commercial service between Moscow and Vladivostok. In addition, television demonstrations took place via these satellites from Moscow to the French ground station at Pleumeur-Bodou, France.

SUMMARY AND OUTLOOK

The capability for providing high-quality communications links for transmitting voice, television, and data traffic between large, sophis-

ticated, and expensive ground stations by satellites has been developed, demonstrated, and reduced to commercial operational practice. The Communications Satellite Corp. is refining and using this capability. In the area of communications satellites, NASA is continuing to develop techniques for satellite communication, using more simplified and inexpensive ground stations with several links in simultaneous use. Progress is also continuing in the use of various frequency bands, such as VHF, for voice communications with aircraft; in the use of frequencies above 10 gigacycles for satellite communications; and in the use of larger, more sophisticated satellites and control systems for conducting several, not necessarily related, technological and scientific experiments on a single spacecraft in the Applications Technology Satellite Program.

SATELLITE GEODESY

J. K. Gleim and Nancy G. Roman

Physics and Astronomy Programs
Office of Space Science and Applications, NASA

Satellite Geodesy

THE ORBITAL PARAMETERS for Explorer XXVII, the Beacon Explorer satellite, shortly after its launch on April 29, 1965, were as follows:

Apogee	1320.5 km
Perigee	931.6 km
Inclination	41°
Period	108 min

The inclination was selected because it would be particularly useful for programs of dynamical geodesy. In order to obtain a detailed description of the Earth's gravitational field, a variety of orbital inclination is desirable. Previous satellites which are contributing to the solution of this problem have had inclinations of 33°, 50°, 67°, and 90°. A modest eccentricity is also desirable to allow a more accurate determination of the angular position of perigee and thus simplify analysis of the results.

Explorer XXVII carries three basic transmitting systems: ionospheric beacons at 20.005, 40.010, 41.010, and 360.090 MHz; Doppler beacons at 161.987 and 323.974 MHz; and a telemetry and tracking transmitter at 136.740 MHz. It also carries a mosaic of corner reflectors on the forward face of the satellite. These reflect laser beams transmitted from ground-based stations. A photodetector is used to determine whether the laser beam has intercepted the satellite; if so, both the direction of the satellite and the delay time are determined. Several groups, including one at the Goddard Space Flight Center, have tracked this satellite by laser reflection for the purpose of developing tracking techniques. Ultimately this may prove to be an unusually precise method of tracking near-Earth satellites. Since no onboard power is required, satellites carrying corner reflectors can be tracked indefinitely. The U.S. Navy Doppler tracking network (Tranet) has determined orbits accurately by tracking the stable transmitted frequencies. Explorer XXIX, GEOS I, was launched from Cape Kennedy on November 6, 1965, as part of the National Geodetic Satellite Program. This is the first satellite launched by NASA expressly for geodesy. The primary objectives of this program are as follows: (1) To connect continental and local geodetic datums in a one-world datum and to relate all surface

datums to the Earth's center of mass, so that positions can be determined in a three-dimensional coordinate system with an accuracy of .10 meters or better; (2) to map with a high accuracy the structure of the Earth's gravitational field; and (3) to compare and correlate results from different instrument techniques so that greater accuracy and reliability can be accomplished. The U.S. Coast and Geodetic Survey and the Department of Defense are also supporting this program.

Explorer XXIX has five types of geodetic measuring systems: (1) A flashing light beacon which can be photographed against a background of stars; (2) quartz cube corner reflectors similar to those on Explorer XXVII; (3) three radio transmitters to provide data for determining the orbit by accurate measurements of the velocity-induced Doppler shift; (4) a radio range transponder to fix the satellite's position relative to that of the interrogating ground stations; and (5) a range and range-rate transponder to determine the range and radial velocity of the satellite. The latter is a system developed by the Goddard Space Flight Center for tracking satellites, such as Eccentric Orbiting Geophysical Observatories and Syncom, in very high Earth orbits.

One feature of the 175-kilogram geodetic Explorer is an 18-meter boom of silver-plated beryllium-copper which provides a gravity-gradient attitude stabilization, so that the optical beacons, laser reflectors, and radio antennas point earthward at all times. Explorer XXIX moves in an orbit with an apogee of 1974 kilometers, perigee of 966 kilometers, inclination of 59.4°, and has a period of about 120 minutes.

The initial phase of the National Geodetic Satellite Program is still underway. In addition to testing the geodetic equipment on board the satellite, all of which appears to be functioning well, John Berbert of Goddard Space Flight Center has begun an intercomparison of ground-based camera instrumentation. Observational procedures and plate-reduction methods have been compared in order to estimate the relative accuracies of each system.

Guier and Newton (ref. 1) used orbital determinations and data residuals from the Doppler tracking of five satellites to deduce values for the zonal harmonics of the Earth's gravity field of odd degrees through the 9th, the nonzonal harmonics of all degrees from the 2d through the 8th, and the sectorial harmonics of 13th degree and order. The zonal and nonzonal harmonics determined from these data are given in tables I and II, respectively. Combining these with values given by King-Hélé for the zonal harmonics of even degree, they computed a shape of the geoid and studied the distribution of the magnitudes of the harmonics. They find no strong relation between the harmonic coefficients of low degree for the geoid and those for the

Table I.—*Values and Mean Deviations of the Zonal Harmonics of Odd Degrees in Units of* 10^{-6}

n	J_n
3	2.676 ± 0.010
5	$.028 \pm .017$
7	$.593 \pm .028$
9	$-.177 \pm .022$

Table II.—*Nonzonal Harmonics of the Gravity Potential in Units of* 10^{-6}

[In each *(n, m,)* pair the A coefficient is listed above the B coefficient]

m	n						
	2	3	4	5	6	7	8
1...............	....	6.90	—2.39	0.64	0.00	0.69	—0.86
		.80	—1.87	—.78	.51	.51	—.28
2...............	7.53	4.56	1.77	1.26	—.82	2.51	.55
	—3.79	—2.54	1.88	—1.58	—.79	.33	—.22
3...............	....	2.47	3.59	.43	2.70	2.16	—.32
		3.66	.03	.49	.26	—1.13	1.26
4...............	....	....	—.89	—2.29	—1.56	—.75	—.40
			.81	—1.22	—2.59	.00	.22
5...............	....	....	....	—.16	—.90	—.31	.47
				—3.14	—2.60	—1.02	.01
6...............	....	....	....	....	.07	—2.49	—.13
					—1.18	4.15	3.88
7...............	....	....	....	....	....	.48	.99
						—.79	—.41
8...............	....	....	....	....	....	......	—.85
							.55

topography. Therefore it appears that the effects which shape the major features of the geoid are the same as those which caused the observed distribution of the continents. In other words, large-scale convection currents in the mantle are not significant in shaping the geoid.

C. A. Wagner (ref. 2) of Goddard Space Flight Center, in a study of the gravity field of the Earth with the aid of Syncom II, found a difference in the major and minor radii of the Earth's elliptical equator of $a_0 - b_0 = 66 \pm 9$ meters. The parameters of equatorial ellipticity as given by the Syncom II data are:

$$J_{22} = -1.7 \times 10^{-6}$$
$$\lambda_{22} = -18°$$

The new results confirm an earlier postulate that higher order longitude-dependent Earth-gravity effects have small influence on the long-term drift of a high-altitude 24-hour satellite. The consistency of the drift data indicates that the Earth is more homogeneous, at least to the third order, than had been supposed previously.

REFERENCES

1. GUIER, W. H.; AND NEWTON, R. R.: *The Earth's Gravity Field as Deduced From the Doppler Tracking of Five Satellites.* J. Geophys. Res., vol. 70, 1965, p. 4613.

2. WAGNER, C. A.: *The Equatorial Ellipticity of the Earth From Two Months of Syncom II Drift Over the Central Pacific.* NASA TN D-3315, 1966.

SATELLITE METEOROLOGY

William C. Spreen, Robert H. McQuain, and
George Tennyson, Jr.

Space Applications Programs
Office of Space Science and Applications, NASA

Satellite Meteorology

INTRODUCTION

THE DOCUMENT entitled "Significant Achievements in Satellite Meteorology, 1958–1964" (ref. 1) reviewed the status of meteorological observations prior to 1958 and described the achievements of space technology in meteorology from 1958 through 1964. The contributions of space technology to meteorology during 1965 and the scientific results published during 1965 based on satellite and sounding rocket data are described in this document. These results mark the program's progress toward the achievement of the objectives outlined below.

Objectives of the Meteorological Program

The overall objective of the meteorological satellite and sounding rocket program is to provide the space technology which, together with more conventional observational techniques, will increase our knowledge and understanding of the Earth's atmosphere, improve our forecasting over extended time periods, and supply a basis for designing weather modification and control experiments. ° This objective provides for a fundamental program which is well suited for expansion to include the systematic exploration of the meteorological characteristics of the atmospheres of other planets. An overall objective such as this lends itself to division into specific objectives for achievement.

Global and Local Observation of Cloud Cover Day and Night

The first and most dramatic application of the meteorological satellite observing system has been the identification and tracking, by means of the characteristic cloud signatures, of known meteorological phenomena such as hurricanes, typhoons, extratropical cyclones, and frontal systems. Thus, the capability is needed for both day and night cloud-cover observations over the entire world. The satellite obtaining the data must be capable of delivering the recorded data (for up to several orbits) to the appropriate command and data acquisition (CDA) stations. A satellite capability must also be provided for obtaining cloud-cover data either day or night and delivering the data

17

to simple, inexpensive ground equipment at a local weather station within line of sight of the satellite. This provides direct readout of the local cloud cover to the local weather station, whereas the recorded data provide world cloud-cover data to the meteorologists responsible for analyzing the entire world's weather.

Global Quantitative Measurement of the Atmospheric Structure and Radiative Flux

Atmospheric disturbances can propagate around the world in as little as 3 or 4 days. To understand and predict the future state of the atmosphere (beyond a day or two), it is necessary to know the initial conditions of the atmosphere over the entire globe including both the thermodynamic structure and the heat budget.

Although the general physical and mathematical relations governing weather prediction have been known for some time and electronic computers could be made available which are capable of handling the huge quantities of data required, the meteorologist has been hampered by the lack of adequate, properly distributed observations. Less than 10 percent of the Earth has adequate observational sites and it is neither feasible nor economical to extend conventional observational techniques into the data-sparse areas. The meteorological satellite provides a means of overcoming this limitation.

Continuous and Variable Time-Scale Observation of Atmospheric Motion and Structure

The size and lifetime of storms are related. The large storms have durations measured in days and weeks, and the small storms, such as thunderstorms and tornadoes, have durations of a couple of hours or less. Also, the longer lived storms may undergo changes in intensity over short time intervals. Polar orbiting satellites cannot provide an adequate frequency of observation for the identification and tracking of local severe storms or for following rapid weather changes. To provide such a capability, the development of a continuous viewing satellite is required. A satellite in an equatorial orbit at synchronous altitude would provide a capability for a continuous variable time-scale view of the tropical and temperate zones of the Earth.

Participation in Weather Modification and Control

By providing information which will improve our understanding of the atmospheric processes, the NASA programs in space sciences and meteorology are assisting in establishing a scientific basis for atmospheric modification. During the next decade it will be reasonable to consider the study and design of experiments and the flight of systems in space modify or control weather locally or even on a regional basis.

Such an experiment would probably involve either the local or regional concentration of, or interference with, solar radiation by space techniques. Spacecraft, either manned or automated, offer means of conducting this type of experiment. However, the experiments will require major advances in technology and in the understanding of the consequences of the solar input.

Whether such experiments are conducted by or in cooperation with NASA, by other agencies, or by other nations, it will be vital to observe the initial state of the atmosphere and the effects of the experiment in sufficient detail. The spacecraft systems implied in the first three objectives are vital to obtaining such detailed observations.

Exploration and Study of the Atmospheric Region Between 30 and 100 km

Rocket measurements, observations of meteor trails, and other phenomena in the region above 30 kilometers indicate that the systematic study of this region is important to our understanding of the overall circulation of the atmosphere. However, regular atmospheric observations of the upper atmosphere made with the conventional balloon-radiosonde technique are limited in altitude to about 30 kilometers. Rocket techniques must be considered for the systematic sounding of the atmosphere above 30 kilometers.

To extend the observational network beyond the existing national rocket ranges, it will be necessary to develop economical, safe, and simplified rocket sounding systems.

The importance of the 30- to 100-kilometer-altitude region is becoming increasingly clear. Large, significant temperature variations measured in this region probably play an important role in the meteorology of the lower regions. From an applications point of view, a detailed knowledge of the variations in this region is required for space vehicle design constraints, for launch, and for reentry.

Planetary Meteorology

Automated and manned exploration of Mars is seen as one of the goals of the future. Data on the Martian atmosphere are important scientifically both in their own right and as guides to the history of planetary bodies. Also, sufficient information must be available to permit manned exploration and operation on the planet. Atmospheric information such as pressure, density and temperature profiles, scale height, and circulation of the atmosphere are necessary for design and operation of spacecraft and equipment.

The first measurements of the Martian atmosphere will be obtained from flyby and individual probes. After these it will be necessary to initiate the systematic investigation of the Martian atmosphere and

the variation of the meteorological elements which characterize the planet's atmosphere. Techniques and experiments for measuring the state and structure of the Earth's atmosphere will undoubtedly provide the basis and experience for developing a means of investigating the Martian atmosphere.

Development of Necessary Techniques and Equipment

The development of the techniques and equipment to fulfill the objectives of the program is the continuing purpose of the supporting research and technology (SRT) efforts. These efforts are divided into sensor and engineering research.

METEOROLOGICAL SATELLITES

Background

Efforts continued during 1965 to determine which meteorological parameters are best measured using satellites, to develop the sensors to make the measurements, to develop methods of collecting data, and to devise methods of using these data in the mathematical atmospheric models.

Meteorological Satellite Program

Two additional Tiros satellites with improved performance and increased capability were successfully orbited in 1965. The data obtained by satellites continue to be widely used by meteorologists for both operations and research.

The meteorological satellite flight program consists of Tiros, the Tiros operational satellites (TOS), and Nimbus. The immediate objectives for these projects continue to be as follows:

(1) Development of satellite system equipment and techniques and satellite launchings directed toward new and improved methods of observing atmospheric meteorological parameters and increased understanding of the atmosphere.

(2) Cooperation with the Environmental Science Services Administration in the establishment and support of an operational meteorological satellite system.

Tiros

During 1965, Tiros VII and VIII continued to operate successfully in orbit and to provide useful meteorological information. Tiros IX was successfully launched in January 1965 and definitely established the feasibility of the cartwheel configuration for an operational satellite. Tiros X was successfully launched in July 1965, and this axial

mode spacecraft, in a sun-synchronous orbit, provided complete coverage during the hurricane season.

Tiros Operational Satellites (TOS)

Considerable progress was made in 1965 in developing and implementing the TOS system. The initial system will employ two types of satellites, one to furnish local users with automatic picture transmission (APT) pictures and the other to provide global pictures remotely to the two command and data acquisition (CDA) stations (ref. 2). The data received at the CDA stations will be immediately transmitted over wideband communications links and used by the Weather Bureau for daily weather forecasts and for research. The data will also be provided to the Air Force at Offutt Air Force Base, Nebr., for operational use. The system will be implemented early in calendar year 1966, with the launches of spacecraft based on the cartwheel Tiros configuration developed in the NASA R&D program. The TOS spacecraft will carry the advanced vidicon camera system (AVCS) to provide global cloud picture coverage and the APT subsystem to provide local readout. Both these camera systems were developed in the Nimbus R&D program. Systems and sensors checked out in the NASA R&D program will be incorporated in future TOS spacecraft.

Nimbus

Nimbus is a three-axis-stabilized, Earth-oriented, research and development meteorological satellite capable of providing full Earth coverage on a daily basis by means of a nearly polar orbit having an inclination of approximately 80° to the equator. The Earth's rotational movement provides the mechanism for longitudinal coverage, while latitudinal coverage is obtained by the spacecraft's orbital motion. The satellite will always view the Earth at nearly local noon on the sunlit side and nearly midnight on the dark side.

The overall Nimbus objectives are to conduct an R&D program aimed at developing and exploiting space technology for meteorological research purposes. The program includes a series of meteorological satellites with improved operating characteristics, and carrying experiments for atmospheric research and for development toward operational use. Measurements will be made of the many atmospheric parameters which are essential to the full description and understanding of the atmosphere. Also it will be useful to measure simultaneously space environmental factors (the solar environment) and the behavior of the Earth's atmosphere, permitting a time correlation of the two.

Results

Achievements in Spacecraft Technology

Tiros IX

Tiros IX, launched in January 1965, was the first spin-stabilized, wheel-mode satellite and was equipped with new magnetic attitude-control coils which established three controllable satellite dipoles or magnetic moments about the satellite axes.

Structure.—The spacecraft is an 18-sided right polyhedral prism, 0.6 meter high and 1.1 meters in diameter, weighing 138 kilograms (fig. 1). The structure consists of a reinforced baseplate and a cover
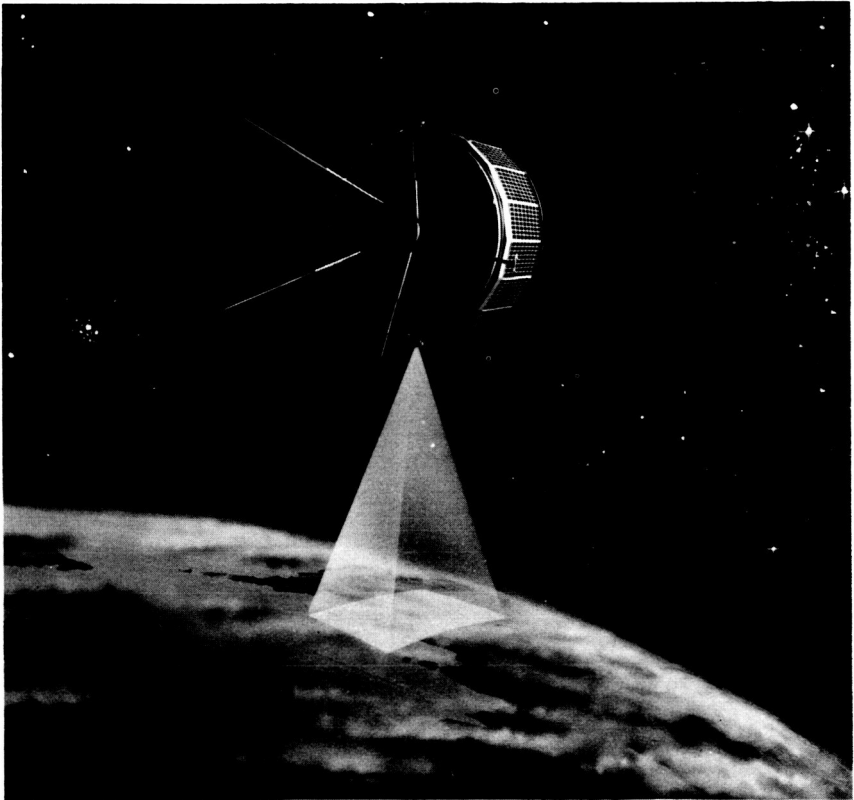
Figure 1.—Tiros IX spacecraft.

assembly. Four transmitting antennas project diagonally from the baseplate and a receiving antenna projects from the cover assembly. The cover assembly has 18 side panels and an upper plate. Two of the

panels have openings for the cameras and two are shortened to accommodate the despin weights. The electronic components are mounted on the baseplate and solar cells are mounted on the top and sides of the cover assembly.

Power Supply.—The power supply, which delivers up to 2.2 amperes, consists of solar cells, storage batteries, voltage regulators, and protective circuits. Solar energy is converted to electrical energy by 9120 N-on-P silicon solar cells, 1 by 2 centimeters, mounted on the top and sides of the cover assembly. The solar cells are arranged in shingles of five series-connected cells with a conversion efficiency of 9 percent at 1.95 volts and a temperature of $27° \pm 2°$ C. During the orbital day, the solar array output is fed directly to the spacecraft subsystems. Current that is not required is used to charge 63 nickel-cadmium storage cells which have a total capacity of 295 watt-hours. During orbital night, the batteries supply spacecraft power (ref. 3).

Attitude Control and Stabilization.—The attitude stabilization and control subsystems orient and spin-stabilize the spacecraft and torque it to the wheel configuration. Spin control is provided by a yo-yo despin mechanism and spinup rockets. Precession damping for spin stabilization is accomplished by two tuned energy-absorption mass (TEAM) mechanisms installed vertically, 180° apart, on the spacecraft inside wall. The TEAM mechanisms are tuned to the precession frequency of the spacecraft and travel up and down monorails in response to the forces generated by the precession of the spacecraft thus damping out initial spacecraft wobble.

The spin-stabilized third stage of the launch vehicle imparts a spin rate of approximately 126 rpm to the spacecraft at separation. Spin reduction to 10 to 12 rpm is provided by the yo-yo despin mechanism consisting of a pair of cable-attached devices affixed at points 180° apart on the periphery of the spacecraft. The yo-yo devices are released approximately 10 minutes after spacecraft separation from the third stage, either by the despin-release circuitry or ground-station command, permitting centrifugal force to unwind the cables. After spin reduction has been accomplished, the cable-attached masses then slip from open hooks and separate from the spacecraft.

Because of the drag effect between the Earth's magnetic field and the magnetic material in the spacecraft, solar radiation pressure, aerodynamic torquing, and internal tape-recorder torquing, the spin rate would drop below the desired 8-rpm minimum after some period of time. To maintain the spin rate within acceptable limits (8 to 12 rpm), two types of spin control device are provided: spinup rockets and magnetic spin control using dynamic control (Dycon) and a magnetic spin control (Masc) coil.

The spinup rockets are five diametrically opposed pairs of solid-propellant rockets mounted around the periphery of the spacecraft baseplate. Each rocket motor develops an impulse of approximately 1.4 pounds per second. When fired in pairs by ground command, the motors provide a 2-rpm increase in spin rate. Two Dycon units provide:

(1) Programed control of the Masc coil currents
(2) Programed control of quarter-orbit magnetic attitude control (QOMAC) coil currents.
(3) Backup vertical drive and shutter control for the cameras.

Each Dycon unit has a pair of orthogonal horizon scanners, one of which is redundant. The output from one orthogonal horizon scanner pair, selected by ground command, provides horizon pulses to spin-synchronize the Dycon operation. A Masc device provides for accurate ground-command control of the spacecraft spin rate. The Masc operates on the principle of a dc motor, in which the armature is represented by the magnetic coil of the spacecraft and the permanent magnet field is represented by the Earth's magnetic field. By reversing the direction of the current in the armature at the correct spin frequency, the interaction of the fields of the core and the magnet generates a maximum usable torque in one direction.

The QOMAC technique is used to correct the attitude of the Tiros wheel in maintaining spin-vector alinement. By programing the direction of a fixed magnitude current through the torquing coil under command of the spacecraft clock, the effective orbit-average Earth's magnetic field vector can be made to lie in the orbital plane and can be made to assume any desired direction within this plane. QOMAC is based upon utilization of the torque developed by the Earth's magnetic field on a spacecraft-contained loop. Since the spinning spacecraft is a gyroscopic body, imposed torques will precess the gyroscopic or spin axis as they would a gyroscope; that is, about an axis normal to the plane containing both the spin and torque vectors.

The magnetic bias control nulls any residual magnetic dipole in the spacecraft after launch and reduces the number of torque cycles required of the QOMAC system by aiding in station keeping. The magnetic bias switch controls the amount of current in the magnetic bias coil and thus its magnetic moment.

The V-head horizon scanner consists of two infrared horizon sensors arranged in a V-configuration. The plane of the V contains the spin axis, and the bisector of the angle between the optical axes is normal to the spin vector. As the spacecraft spins, the optical axes trace two cones in space. If the spin axis of the spacecraft is normal to an Earth

radius, the outputs of the sensors are identical. If a yaw error exists, there will be a roll error 90° later in orbit because of the inertial rigidity of the spin vector. This roll error is detectable.

Television Subsystems.—The camera subsystems consist of two identical ½-inch (0.01 meter) vidicon cameras. The optical axes, instead of being parallel to the spin axis, as they were in previous Tiros spacecraft, are inclined approximately 26.5° to each side of the plane of rotation. The cameras operate in two modes: a storage mode for picture taking over remote areas and a direct readout mode for picture taking within range of the CDA station. For the storage mode, a CDA station will transmit commands to the spacecraft to cause the camera to photograph a prescribed remote area. In this storage mode, a maximum of 48 pictures may be stored on each magnetic tape recorder for readout when the spacecraft passes within range of a CDA station. For the direct readout mode, the tape recorder is bypassed and the CDA station receives the pictures as they are read off the vidicon. The cameras have 104° wide-angle lenses, with a resolution of 3.33 kilometers at the subsatellite point. Each wide-angle camera is configured to take 16 pictures per orbit (at 128-second intervals) to give nearly dawn-to-dusk coverage. The total pictures per day for both cameras would then be over 450. The TV tube is a 500-scan-line vidicon with a persistence that permits a 2-second scan with less than 20-percent degradation in picture quality.

Tiros X

Tiros X, a conventional Tiros similar to Tiros VI, was launched on July 2, 1965, into a nearly polar, nominally 740-kilometer, nearly circular, Sun-synchronous orbit, 81.6° retrograde, with an orbital period of 99.6 minutes. The orbital plane precesses easterly about 1° a day, at the same rate as the Earth-Sun line. The spacecraft crosses the equator at 10:45 a.m., local time, to acquire maximum solar power and to provide optimum illumination. The 131-kilogram spacecraft carries two wide-angle ½-inch (0.01 meter) vidicon cameras, positioned parallel to the spin axis (ref. 4).

The basic changes from Tiros IX are that Tiros X has no provision for command-confirm and no V-head scanners, which were required by the wheel configuration.

Nimbus

Spacecraft Configuration.—The Nimbus I satellite, in its 26½-day flight, established the operating feasibility of virtually all its basic systems in the space environment. Many of these systems will continue to be used in similar modes of operation for ongoing Nimbus spacecraft. Furthermore, Nimbus I has given evidence that the spacecraft per-

formance goals outlined in reference 1 can be more than minimally achieved through the use of this general type of spacecraft configuration. The major spacecraft elements are described in reference 1 and shown in figure 2.
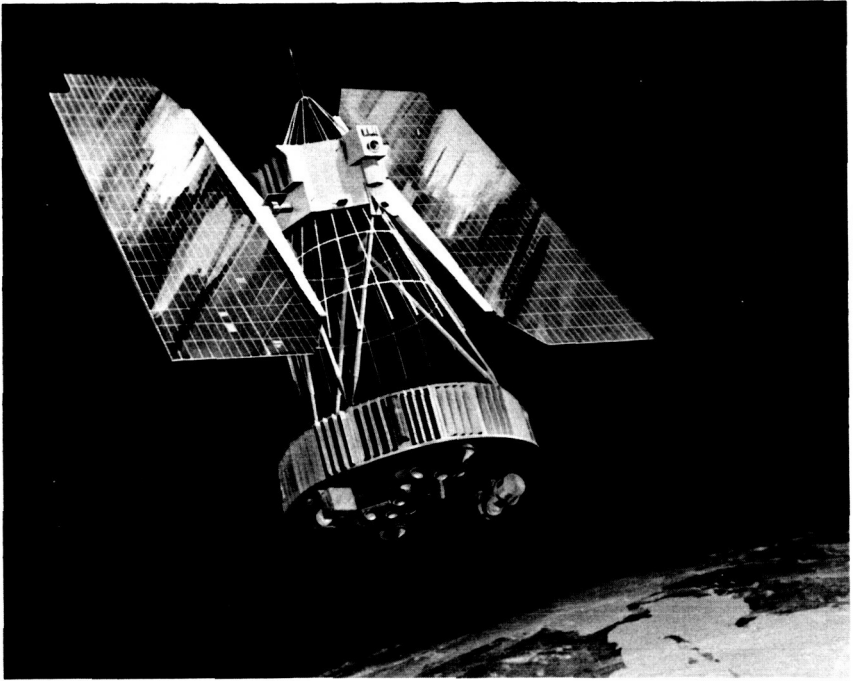
Figure 2.—A Nimbus series spacecraft.

Nimbus C, the second flight spacecraft, is scheduled for flight next year. The bulk of its integration, environmental evaluation, and performance verification procedures were successfully completed during 1965. This spacecraft will include a capability for the direct readout of nighttime cloud pictures by combining the high resolution infrared radiometer (HRIR) systems with the transmitting and receiving elements of the automatic picture transmission (APT) system, and the addition of a medium resolution infrared radiometer (MRIR) sensor to obtain data on the Earth's heat balance.

Improvements have been made in the reliability, performance, and life characteristics of the advanced vidicon camera system (AVCS) and the APT television sensors.

The Nimbus B spacecraft is scheduled for launch in calendar year 1967, and will include seven meteorological experiments in place of the four on Nimbus C.

Stabilization and Control.—The Earth-oriented, Sun-synchronous Nimbus I satellite satisfactorily achieved attitude stability about its three axes. Continuing attitude control was actively sustained, generally within 1° about each axis, by closed control loops which corrected attitude errors by the application of pneumatic torquing and flywheel action. A separate control loop maintained Sun orientation of the large solar paddles during the daylight orbit.

While the Nimbus I control system performed surprisingly well after being launched into an elliptical instead of a circular orbit, some modifications were designed during 1965 to improve the stability and life of the next Nimbus spacecraft. The most significant changes are redesign of the solar array drive subsystem and corrections to the pitch (orbital direction) and roll (orbit-perpendicular) pneumatic controls. The former task provided a substantially improved design of solar paddle control mechanism over that of Nimbus I, a design which satisfactorily completed all tests including a life-test demonstration of 4000 hours in a simulated space environment. The pneumatic changes will provide finer control of the gas nozzles during coarse attitude adjustments, thereby reducing gas consumption and preventing the buildup of overcompensating torques about the pitch and roll axes.

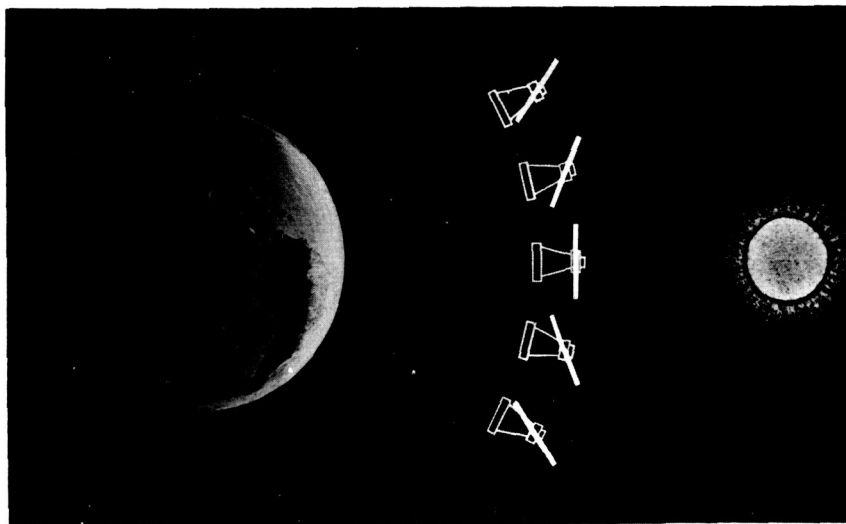Figure 3 illustrates the desired orientation of the solar paddles

Figure 3.—Nimbus solar paddle orientation.

toward the Sun. The Nimbus I solar array drive slowed down and stopped after 26 days in orbit. An intensive investigation followed in

Figure 4.—Nimbus HRIR strip showing effects of roll error.

which the increasing frictional drag was traced to an excessive accumulation of heat which was increasing the viscosity of the bearing lubricant. This demonstrated the predominant failure mode of the solar array drive, and ultimately of the spacecraft. The redesign of this drive effected significant motor-bearing temperature reduction and incorporated greater potential torque capability. This culminated a joint research endeavor between NASA, its spacecraft contractor, and some leading national authorities on the behavior of bearing lubricants (ref. 5).

It has been previously noted in reference 1 that Nimbus I exhibited attitude errors in excess of 1° in pitch and roll, and above 2° in yaw during part of the orbit. For example, an analysis of some HRIR scenes and of the appropriate telemetering record shows 3.5° of roll error. The blips on the horizon of the HRIR data in figure 4 show the means of making this measurement.

Power Supply.—The Nimbus I power system derived its electric energy from solar energy incident upon 11 982 silicon solar cells located on one side of the two honeycomb-contruction paddles. An additional battery was added in 1965 to Nimbus C to support day-and-night operations of an added MRIR experiment (ref. 6).

Sensor Subsystems.—Nimbus I meteorological sensors have shown that collection and transmission of infrared and television cloud scenes could be accomplished with high accuracy, resolution, and clarity. Nimbus I also established very significant advances in data coverage and utilization. Specifically, the HRIR has provided a way to measure thermal emission from land and sea surfaces and to map nighttime cloud cover. The AVCS provided a wider geographical coverage and higher image resolution than previous meteorological-satellite systems.

A second prominent television-type cloud sensor was the APT system with the practical provision of a continuing daytime readout of cloud coverage to local ground viewers. The success of this principle and its interesting implication to international weather data utilization have spurred later efforts toward similar provisions for sending HRIR data on the same real-time transmission link in Nimbus C and follow-on spacecraft.

The Nimbus C sensors (fig. 5) which were flight qualified in calendar year 1965, have been prepared and somewhat modified for the upcoming flight. Some of the important sensor changes are as follows (ref. 6) :

(1) *Medium resolution infrared radiometer (MRIR)*.—The MRIR is a five-channel radiometer that provides data on the emitted and reflected radiation of the atmosphere and Earth's surface in five spectral bands:

Channel 1—Water-vapor absorption band, 6.5 to 7 μ

Channel 2—Atmospheric window, 10 to 11 μ

Channel 3—Stratospheric temperature, 14 to 16 μ

Channel 4—Terrestrial radiation, 5 to 30 μ

Channel 5—Albedo, 0.2 to 4 μ

These data will be obtained with a resolution of about 48 km. This sensor receives radiation by means of a rotating mirror that scans the Earth perpendicular to the orbital track. Its instantaneous field of view is 2.85° with a resolution of 47.8 kilometers at the subsatellite
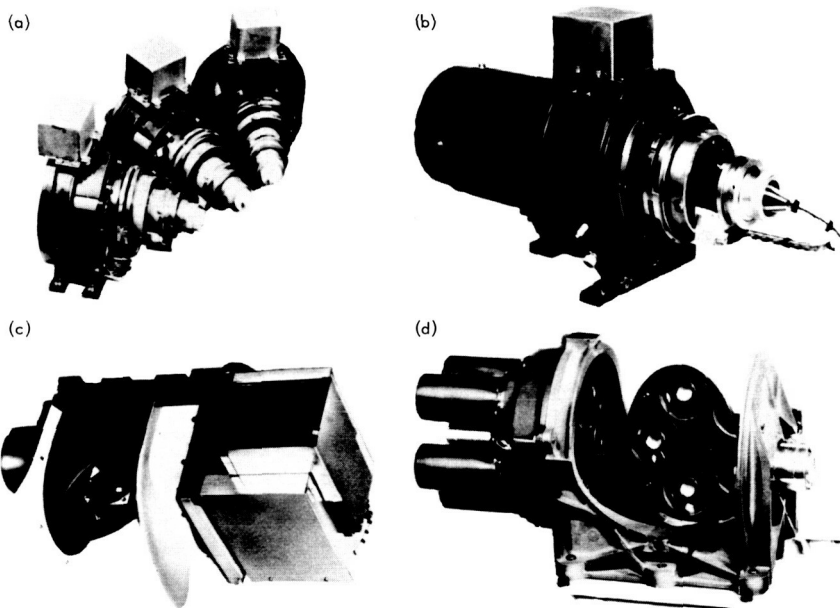
Figure 5.—Nimbus C sensors. *(a)* AVCS; *(b)* APT; *(c)* HRIR (direct and stored); *(d)* MRIR, 5-channel (heat budget).

point. The data from five channels are digitized and stored on parallel tracks of an 80-meter endless-loop tape recorder that is being added to Nimbus C specifically for MRIR use. This digital system will preserve much higher data accuracy than its analog counterpart on Tiros.

(2) *High resolution infrared radiometer.*—Improved shielding will minimize radio frequency interference on the HRIR video data when the APT is operated, giving a clearer picture.

(3) *Advanced vidicon camera system (AVCS).*—The camera iris set-

ting has been refined to correct the picture variation with latitude. Previously, it was optimized only for the equator. The correct exposure is now obtained over the entire orbit.

(4) *Automatic picture transmission (APT).*—The storage vidicon tube has a tremendously increased life characteristic, showing 1000 hours of operation (equivalent to 6 months) without appreciable degradation. The former end-of-life expectancy was 150 to 200 hours. The dynamic picture range has been increased from 10:1 to 25:1, with a commensurate increase in signal-to-noise level.

Performance.—The Nimbus I satellite had 3 weeks of useful flight in August and September of 1964. Its design objectives and initial performance were presented in reference 1. Further knowledge has been gained from postflight studies and particularly from an extensive investigation of the solar array drive system which malfunctioned and terminated the useful life of the satellite.

Following up on the investigation of the Nimbus injection into an orbit with an eccentricity of 0.036, the Lewis Research Center found that the Agena stage lost about 20 kilograms of fuel because of a malfunction in the ground propellant loading system. Because of the shortened Agena burn which resulted, several orbital passes were required for the Nimbus ground station to lock onto the satellite (ref. 7).

The Nimbus I performance, in terms of quantities of data which have undergone various degrees of documentation, cataloging, archiving, and dissemination to users, includes the following totals:

(1) 194 high resolution infrared radiometer HRIR swaths, each scene 6400 kilometers wide and theoretically reaching from pole to pole.

(2) 11 200 advanced vidicon camera (AVCS) pictures, each 800 kilometers by 2400 kilometers.

(3) 1607 automatic picture transmission APT system photographs obtained by 42 different ground stations, each picture was approximately 1600 by 1600 kilometers.

Further results of Nimbus I performance are shown below (ref. 8):

(1) All major objectives of a detailed spacecraft-activation sequence used to determine the system response to various operating modes were fulfilled as planned.

(2) Spacecraft housekeeping telemetry was received and analyzed at Goddard Space Flight Center (GSFC) in real time (at orbital periods), and corrective actions as required were initiated through Rosman and Gilmor CDA ground stations. Remote command of the spacecraft

using the Rosman and Gilmor command transmitters and the command console at GSFC was demonstrated successfully.

(3) Spacecraft time remained within 1 second of ground standard time for more than 612 hours; of approximately 5000 commands, 4974 were executed.

(4) Thermal control maintained average sensory-ring temperature at 22° to 25° C. These temperatures were well within the desired limits for operation.

(5) The solar array produced an average of 13 amperes, which was according to design specifications. Battery voltages were maintained within specifications by the use of auxiliary and compensating loads.

(6) Beacon power did not degrade. Auroral effects, however, were apparent on data received at Gilmor but not at Rosman. Spacecraft tracking records for all Gilmor passes showed evidence of auroral effects. Of the 375 Nimbus I orbits, 208 passes scheduled at Gilmor, 115 passes indicated aurora interference. All of the interference was seen on the 136.5 Mc tracking records; no interference attributed to aurora was found on the wideband 1700 Mc S-band records.

(7) Spacecraft-separation and paddle-deployment maneuvers were executed as programed. Spacecraft stabilization occurred within the first Sun acquisition. Earth orientation was maintained despite an orbit with an eccentricity beyond design specifications. Occasional pitch oscillations resulted from pneumatic impulses exceeding desired values.

(8) The feasibility was established for complete HRIR surveillance of surface features on a global scale at nighttime.

(9) An outstanding capability has been demonstrated for detecting temperature gradients over the Earth's surface in clear-sky conditions.

(10) Observations over the poles revealed the structure and pattern of ice cover, thus demonstrating the applicability of high-resolution radiometry for other scientific disciplines such as glaciology, geology, and oceanography.

Satellite TV Pictures

Introduction

During 1965 the meteorologist was provided with almost complete global cloud-cover pictures on a daily basis for the first time. Tiros VII and VIII continued to provide usable pictures during the year, and Tiros IX and X provided, for operational use, pictures of polar regions; such pictures had been lacking prior to the launching of polar-orbiting satellites. Over 500 000 TV pictures have been provided since the launch of Tiros I in 1960.

The Nimbus 1965 achievements in television pictures included a further interpretation of the Nimbus I pictures, an extended description of the subsequent meteorological and nonmeteorological data utilization, and determination of satellite and camera sensor performances. Numerous investigations were conducted and studies presented on the massive collection of data indicated in the earlier section on Nimbus performance. Two of the best sources of data are the Goddard Space Flight Center publications: *Nimbus I Users' Catalog; AVCS and APT,* and *Nimbus I High Resolution Radiation Data Catalog and Users' Manual,* dated March 1965 and January 15, 1965, respectively (refs. 9 and 10).

Cloud Observations

Tiros IX.—In 1965, Tiros IX, the first wheel-mode satellite, was launched into a nearly polar orbit. With the launch and successful orbit of this satellite, the Environmental Science Services Administration (ESSA) was provided for the first time a view of the entire Earth's weather on a daily basis. With the Tiros data, ESSA routinely prepared daily global cloud maps for use in operational weather analysis and forecasting. Figure 6 is a montage showing the world's cloud formation during a single 24-hour period.

Tiros X.—Tiros X, the first ESSA-funded satellite, was launched in July 1965. This axial-mode satellite was launched primarily to insure satellite coverage during the 1965 hurricane season. This spacecraft was launched into a nearly Sun-synchronous orbit. Its drift out of Sun synchrony is on the order of only 2° per year. Tiros X, together with Tiros VII, VIII, and IX, has provided complete coverage during the hurricane season and has played a significant part in the support of the Gemini V, VI, and VII missions. Figure 7 shows Hurricane Betsy on September 5, 1965. Of particular interest is the size of the eye which was larger than any observed previously by satellite and appeared to be related to the extensive damage associated with this hurricane.

Nimbus I.—The outstanding success of Nimbus I was a result, in no small part, of the performance of improved and directly transmitting types of television cameras, i.e., the AVCS and the APT systems, respectively.

Although an elliptical satellite orbit (perigee of 423 kilometers, apogee of 933 kilometers) resulted from a launch-vehicle malfunction, the orbital path planned was inclined in order to cause a precession of the orbit that was synchronous with the Earth's revolution around the Sun. This permitted an almost constant relationship between the orbit and the Sun during the picture-taking life of the satellite. As a

Figure 6.—Tiros IX cloud montage; the first complete view of the world's weather.

Figure 7.—Hurricane Betsy.

result, the satellite covered most areas of the world twice every 24 hours, approximately at local noon and local midnight. The stored data were read out to two ground stations upon command, Rosman in North Carolina and Gilmor in Alaska.

Of the 14 to 15 orbits completed in a 24-hour period, 11 were expected to be within readout range of one of the two stations. Despite the reduction of orbits within readout range of the ground stations to fewer than 10 per day, because of the eccentric orbit, daytime and nighttime photographs were obtained covering over 50 to 75 percent of the world on a daily basis. Some idea of the enormous amount of data that was available during the Nimbus I operating life can be obtained by considering that the spacecraft processed more than 50 million data words of information per orbit. The great majority of these data was from television pictures.

The pictorial presentations of Nimbus I observations were usually available at the NASA Nimbus Control Center in Greenbelt, Md., within 30 minutes after the command for playback was given. As part of the process of preparing the data for ground use, the observational

data were transmitted to the ground station, recorded, and transmitted by communications circuits to Greenbelt, where latitudinal and longitudinal grids were automatically added and the data were transcribed onto 70-millimeter photographic film.

The width of coverage of one swath varied along the orbit, being generally greatest near high southern latitudes that corresponded to the apogee portion of the orbit during active satellite operation. The maximum AVCS swath width was about 1555 kilometers and the minimum swath width was 600 kilometers during perigee. Reference 9 gives the daily coverage maps chronologically by international day from August 28, 1964, through September 22, 1964, the period of useful Nimbus data.

Nimbus I AVCS pictures are available to research in 70-millimeter transparencies or paper copies. The AVCS format presents successive pictures from each camera on separate filmstrips, with the image area of each picture about 0.5 meter square. A very good example of this data format is in the developed picture sequence of AVCS triplets on the left-hand side of figure 8 for orbit 80/81 which took place on September 2, 1964. The swath proceeds from northernmost Antarctica up through the eastern Pacific Ocean, headed for Alaska. On the right-hand strip is one of the significant simultaneous daytime portrayals of high resolution infrared data. This example is presented to provide the opportunity to compare the relative coverage areas and apparent resolution for these two Nimbus sensor systems.

Automatic Picture Transmission (APT).—The APT camera, though of lower resolution than the AVCS, was able to retain a latent picture image long enough on its photosensitive surface for the image to be directly transmitted to the ground without intermediate storage on magnetic tape. The resolution was still good enough to recognize cloud and terrain features of less than 4 kilometers in diameter. Like the AVCS, the APT formed television images during the day. Quality of the APT data was highly satisfactory, with only slight degradation because of radio frequency interference.

Scientific Results

The operational use of satellite cloud pictures is continually being expanded. They were used. at first, for comparison with conventional analyses, then as confirmation data, and, finally, as direct input to the master analyses for the Northern Hemisphere (ref. 11). During the hurricane season, cloud pictures are used to locate, track, and estimate the intensity of these tropical storms. The first studies were directed toward interpretation and analysis because the data were a completely
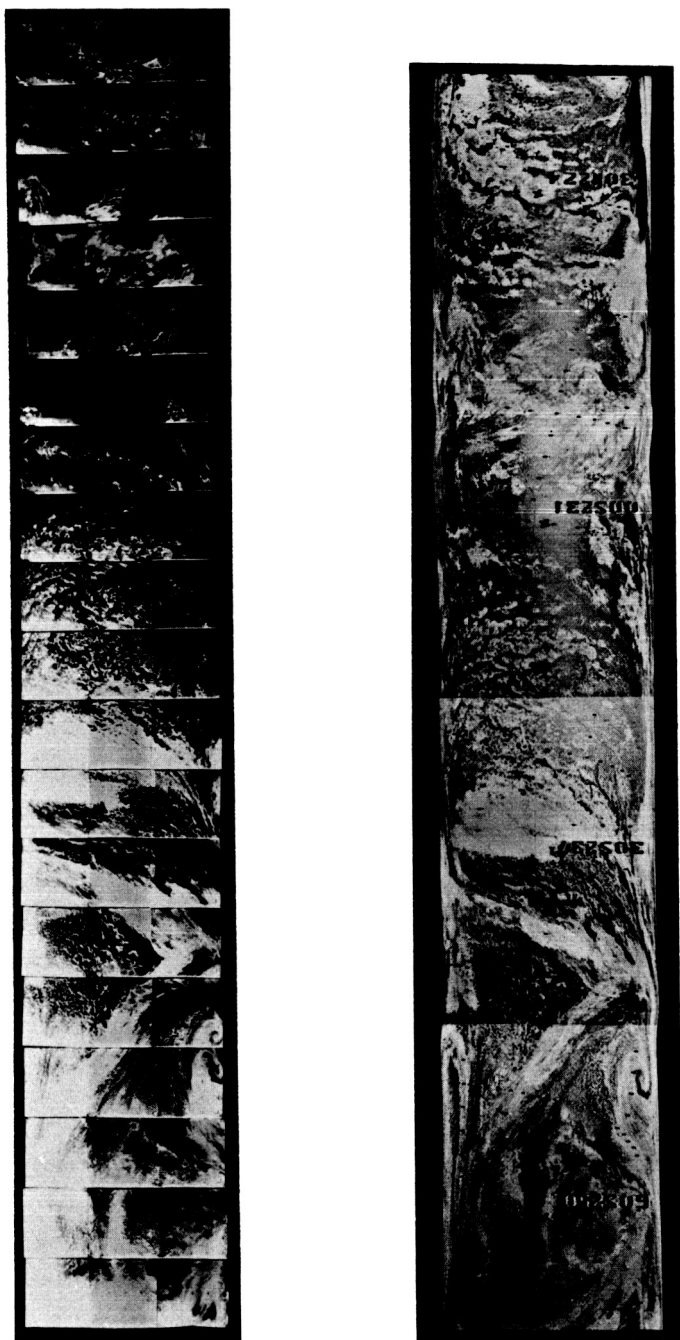
Figure 8.—Nimbus I AVCS (left strip) and daytime HRIR (right strip) comparison; orbit 80/81.

new form of information. Now, the research is directed toward devising methods of extracting maximum information from the satellite cloud data. The areas of study are diverse and include supplementing conventional data, jetstreams, input to numerical experiments, windspeed in the troposphere, and cloud and terrestrial albedo.

Cloud Cover and Storm Development.—Several different, though related, theories or explanations of cyclogenesis are in current use by forecasters to anticipate new storm development. Since cyclogenetic activity is closely related to the three-dimensional motion of the atmosphere, specific cloud patterns could very well indicate conditions suitable for cyclogenesis to occur. The identification of such cloud patterns from satellite data would be a useful technique. Reference 12 is an attempt to deduce probable cloud patterns associated with cyclogenesis in the Gulf of Mexico. The characteristics are illustrated as a sketch in figure 9. The open, unstable cyclonic wave in the Gulf of Mexico is similar to the classic model with a sharply defined, bulging, bright cloud mass on the frontal cloud band and the leading edge of the cold front clearly evident. The bright area is in the vicinity of

Figure 9.—Illustration of features associated with frontal wave model often observed over and near the Gulf of Mexico.

the wave crest and is probably where the newly created area has a maximum of rising motion. In addition, there are two other features. One is the broken appearance of the clouds just behind the leading edge of the cold front, and the second is the area of convective activity some few hundred kilometers ahead of the cold front. These latter clouds are sometimes more organized and appear as a narrow squall line.

Not all storm development takes place as the simple unstable wave phenomenon just described. Another is the development of a new storm over the gulf as an already-occluded system moves into the area (ref. 12). The features of this are a quasi-stationary front extending across the gulf into Texas or northern Mexico, and an approaching Pacific occluded front, or, more generally, an approaching shortwave trough, accompanied by an appreciable region of strong cyclonic vorticity advection at upper levels. The identification of these waves, often initially with the aid of the Tiros data, provides the first indication that the front is becoming quasi-stationary. At this time, the cloud pattern may be similar to that of the open wave. A significant part of the energy for intensification over or near the gulf is derived from a high-level positive-vorticity advection impulse accompanying the occluded front. Adequate indication of this impulse usually is present in the Tiros pictures in terms of cloud patterns identifiable as associated with the occluded front and its corresponding high-level vorticity advection maximum. A suggested schematic of the appearance of a satellite picture taken several hours before initial intensification is presented in figure 10. The quasi-stationary gulf front is shown in the lower portion of the sketch and the cloud mass associated with the approaching Pacific front and vorticity maximum is shown to the upper left.

During the period September 10 to 17, 1963, two eastern Pacific tropical cyclones, Jennifer and Katherine, were located. Jennifer was tracked during September 10 to 12, 1963, after which it moved westward into an area of no data-recording facilities and was lost. On September 17, tropical storm Katherine was located and on the same day caused heavy rains and considerable crop damage over portions of southern California and Arizona. On the basis of ships' logs, synoptic observations, and Tiros VI and VII data, it appears that Jennifer and Katherine were the same cyclone (ref. 13). In retrospect, it appears that this cyclone had a history as early as September 8 when it was a recognizable disturbance near the Gulf of Tehuantepec. Figure 11 is a composite of the earliest information. The Tiros photograph for September 8 (upper left) reveals a large cloud mass near the horizon toward the east. The high oblique view pemits only a crude estimate of the center of the cloud mass. A spiral structure within the cloud mass may exist but is

Figure 10.—Schematic of cloud distribution associated with incipient cyclogenesis as it would appear from a satellite.

questionable. Photographs for September 9 (upper right) show a cloud mass but no suggestion of spiral structure. On September 10 (lower right) the clouds are more organized with evidence of spiral structure. These high oblique Tiros views would not necessarily signify a storm by themselves, but the log of a ship in the area recorded a 17 km/sec wind at 0000 GMT, September 10 (fig. 11, lower left). The combination of data indicates a cyclonic disturbance that was barely tropical-storm strength. For a study of the storm develop-

ment and movement, neither conventional data nor satellite photographs alone are sufficient, but in combination this information makes it evident that Jennifer and Katherine were the same storm.
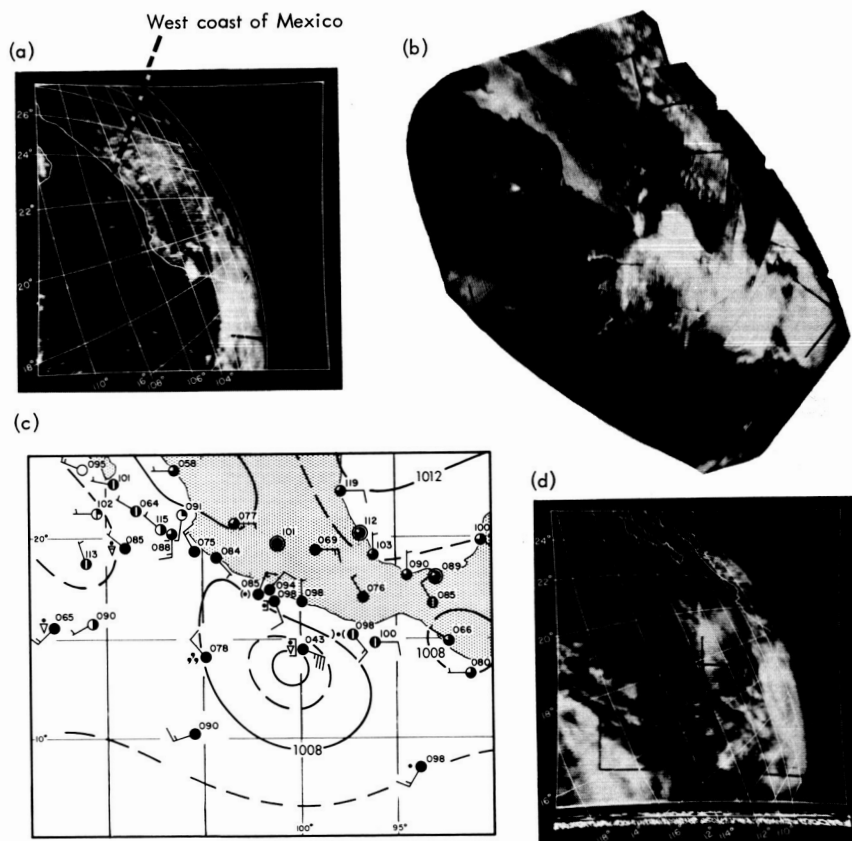

Figure 11.—Tiros VI and VII photographs of the area southwest of Mexico on September 8–10, 1963, showing disturbance near the eastern horizon. (*a*) September 8, 2109 GMT; estimated center, 13° N, 96° W. (*b*) September 9, 1953 GMT. (*c*) September 10, 0000 GMT; surface analyses over same area. (*d*) September 10, 2051 GMT; estimated center, 14° N, 104° W.

Crossover of Jetstreams.—A study by Oliver et al. (ref. 14) described dark bands in Tiros V and VI cloud photographs which were associated with jetstreams at tropopause level. It was concluded that the dark bands were shadows cast by high-level cirrus associated with a

jetstream (fig. 12). The observed cloud distribution was attributed to the merging and subsequent splitting of the polar front and subtropical jetstreams according to the generally accepted relation between cirrus clouds and the jetstreams. However, a further study (ref. 15) of the cloud photographs in conjunction with the analysis of air trajectories
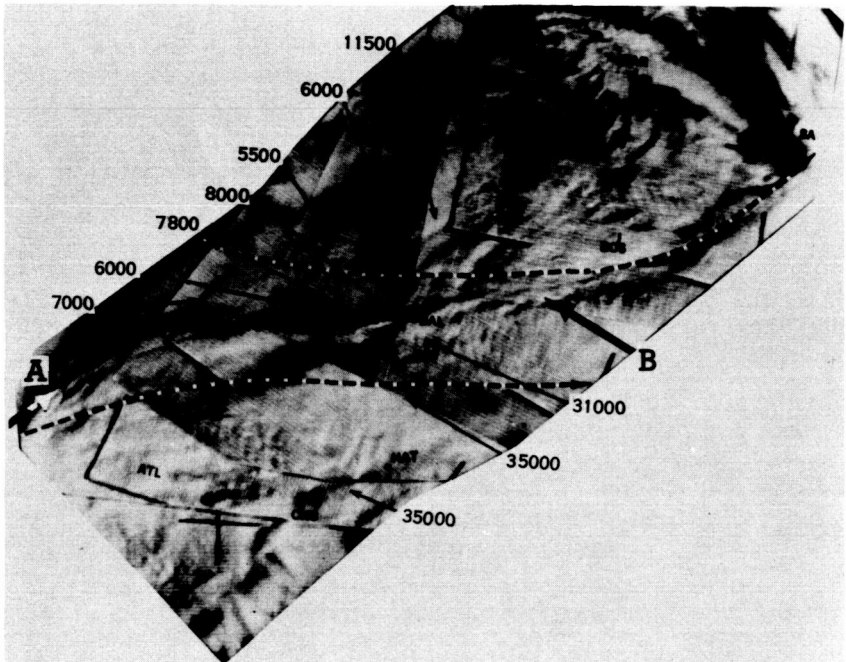
Figure 12.—A mosaic of Tiros VI pass 0922 with cloud-top heights in feet as reported by pilots within 1 hour of picture time. The dashed lines are the position of the jetstream at 200 millibars.

along isentropic surfaces and clear-air-turbulence reports indicated that the classical model of the confluence and difluence of the polar front and subtropical jets with the cirrus clouds on the anticyclonic side of the flow was not supported by the cloud distribution. In this analysis, it appears that the air in the northwesterly jet branch submerges beneath warm air that is traveling within the southwesterly jet. This submergence occurs along a well-developed convergence line marked by a sharp wind-velocity change. The southwesterly jet overrides the northwesterly one, and the air within it follows an ascending motion. With this type of motion, the apparent discrepancy in the cirrus cloud cover can be resolved, for the observed high-level cloudiness remains on the anticyclonic side of the flow.

Numerical Experiments With Satellite Pictures.—Almost from the beginning of Tiros I, it was apparent that large-scale cloud patterns reflected the field of motion in which they were embedded and provided qualitative information about the flow. However, an experiment (ref. 16) was conducted on the derivation of quantitative information on the horizontal field of motion from satellite television pictures. The experiment was conducted over a tropical area by using an IBM 7090 computer program to improve upon the horizontal velocity field, initially estimated from the cloud pictures by also estimating the direction and vorticity patterns.

The cloud pictures show the results of vertical motion and not divergence per se. For that reason, synoptic models and similarly documented flow regimes were used to estimate divergence from the photographic evidence. This experiment was concerned with the lower troposphere where convergence produces upward motion, and the estimates of vorticity and convergence were based on values that appeared reasonable in the light of work found in the literature and the preliminary construction of several hypothetical cases. These established approximate bounds. In the experiment, the main features of the circulation were reasonably well verified and the windflow in the vicinity of the vortex center was correctly indicated. This suggests that the essential elements of the horizontal flow pattern result from a proper combination of vorticity and divergence even though the magnitudes are only approximate. That is, if estimated magnitudes of those fields are correct within a factor of 2 or 4, the essential features of the flow may be retrieved.

More directly related to the day-to-day predictions is the development of techniques for incorporating information derived from satellite cloud pictures into the operational numerical analysis, into data-sparse analysis, and into modification of the 500-millibar stream function analysis or its derivative, the Laplacian field. Two steps are involved. The first is to infer information about the 500-millibar flow pattern or about the large-scale, midtropospheric vertical motion from the cloud patterns photographed by the satellite. The second step is to translate this information into terms that permit modification of the initial 500-millibar analysis where there appears to be an inconsistency between the flow pattern and the cloud pattern. The first step involves the relation of satellite-viewed patterns to the wind and weather systems analyzed on surface and upper-air charts. The second step involves adjustments of the 500-millibar field such as the introduction or repositioning of a circulation center, the altering of the direction of flow in a region, and the relocation of the axis of maximum wind.

The application of the procedure has been completed and docu-

mented for six case studies with all the reanalyses being performed in regions of sparse data; namely, the Pacific Ocean. These first attempts to improve the initial operational analysis by the use of satellite information have shown positive results. Percentage improvements in the root-mean-square forecast errors of the geostrophic wind vector varied from 1 percent to 15.5 percent, and averaged 5.4 percent. In addition, the experience gained by associating Tiros-viewed cloud patterns with corresponding flow patterns at 50 000 N/m^2 will provide a basis for continued development of these techniques.

Wind Fields in the Troposphere.—While the numerous pictures of tropical storms, hurricanes, and typhoons, taken by the Tiros Satellite, have been used in the locating and tracking of these storms, attempts have been made to extend the utility of these pictures to the estimation of the maximum windspeed associated with the storm. This is especially useful in the data-sparse areas (ref. 18). The windspeed estimate is based on the size of the cloud area and the organization of the clouds associated with the storm. The size of the storm is measured by the diameter of the overcast circle which can be drawn around the dense cloud shield of the storm. The degrees of cloud organization exhibited in the bands are classified into four categories ranging from the weakest to the strongest. These four categories are illustrated in figure 13. After the diameter of the overcast circle and the category are determined, the relationship shown in figure 14 is used to estimate the maximum windspeed. This method was tested during the last 6 months of 1964. In 27 test cases where both satellite pictures and reconnaissance-aircraft wind measurements were available, the average departure in windspeed determined by use of satellite pictures was 15 knots (8 m/sec) and the maximum departure was 25 knots (13 m/sec). This technique is now being used operationally (ref. 11).

In a number of situations the cell patterns of convective clouds observed in Tiros photographs have exhibited a relation to the low-level wind field (ref. 19). These situations occur only with patterns composed of clouds formed by convection in the lower levels of the atmosphere. The pattern assumed by a group of convective cells tends to be determined by the wind shear. With no shear, there is a random distribution of polygonal cells, and as the shear increases, the clouds appear as rows, at first transverse to the wind shear but with large shears parallel to the wind-shear vector. The wind at any level is related to the mean wind shear. On this basis Rogers (ref. 19) suggested a classification of windspeed and cloud pattern as seen in the Tiros pictures. The five classes described below, are illustrated in figure 15.

Windspeed 0 to 7 knots (0 to 3.6 m/sec): polygonal cells.—In this speed range, the cumuliform pattern is of randomly distributed regular polygons. Direction cannot be inferred.
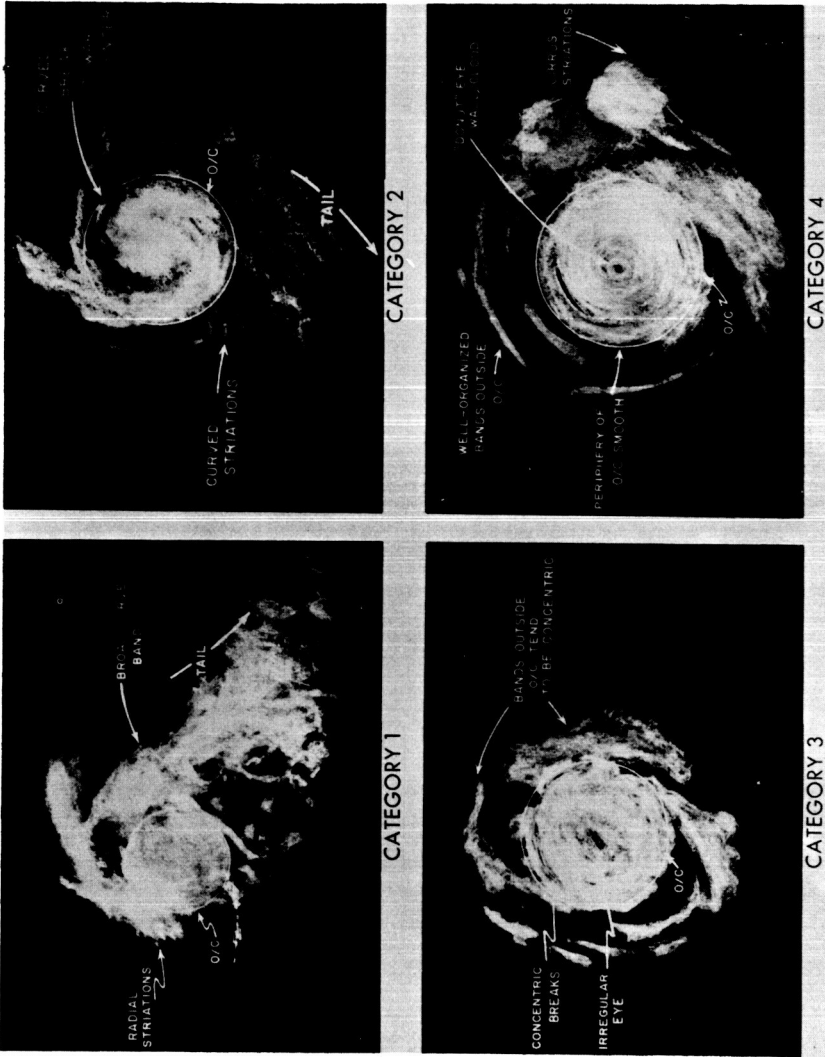
Figure 13.—Schematic illustration of the major characteristics of the four pattern categories.
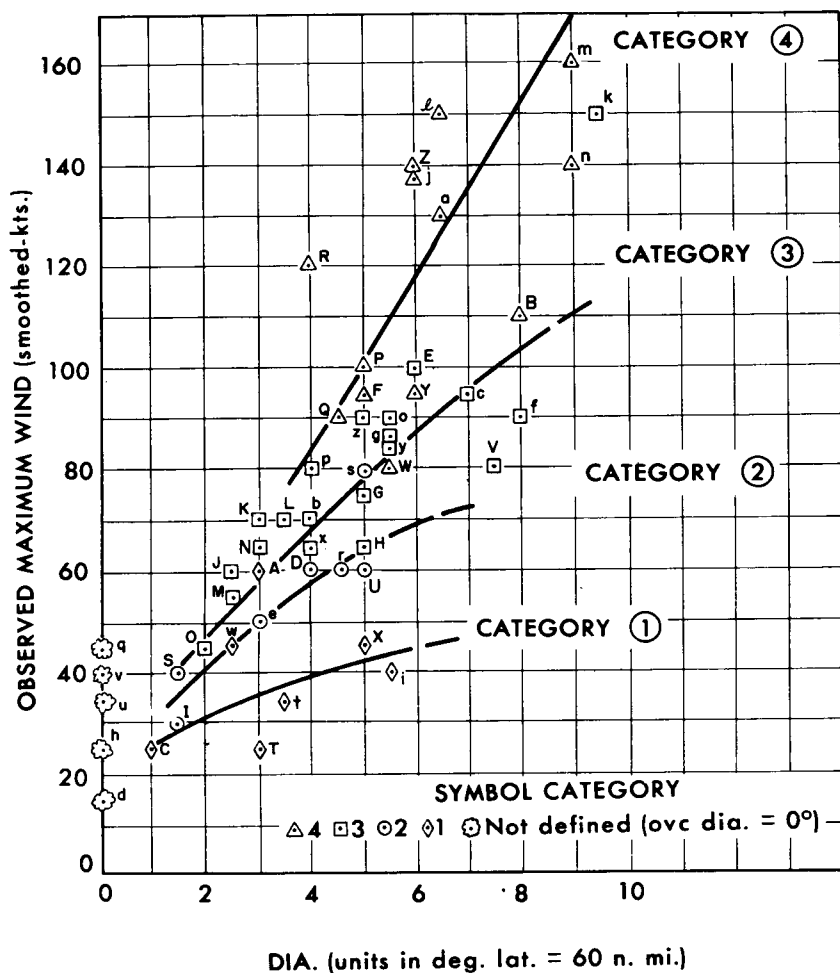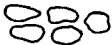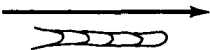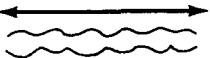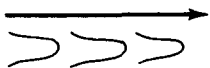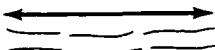
Figure 14.—Maximum windspeed versus diameter of overcast circle, with category isopleths.

Windspeed 8 to 22 knots (4.1 to 11.3 m/sec), lower range: elliptical chains.—At the lower speed range the cells are distorted into ellipses which tend to form a chainlike pattern. The wind direction is parallel to the major axis of the chain and blows from the open to the closed end of the ellipse.

Windspeed 8 to 22 knots (4.1 to 11.3 m/sec), upper range: scalloped.— At the high speed, there is a scalloped pattern of chainlike clouds but the crosswind links are missing. The wind is parallel to the axis of the chain, but there is an ambiguity of 180°.

Cell Pattern		Wind Speed Range
a. Regular polygonal cells		0–7 Knots
b. Elliptical chain		8–22 Knots, lower range
c. Scalloped, with crosswind links missing		8–22 Knots, higher range
d. Blown-out ellipses		23–37 Knots, lower range
e. Rows		23–37 Knots, higher range

Figure 15.—Relationship between wind velocity and cumuliform cellular patterns. Sketches illustrate cloud patterns observed in Tiros photographs. Arrows indicate wind direction inferred from cloud pattern.

*Windspeed 23 to 37 knots (11.8 to 18.0 m/sec), lower range: blown-out ellipses.*—In the lower end of this windspeed range, the patterns appear like blown-out ellipses which have an open end; the ellipses are no longer joined together in a chain. The wind is parallel to the major axis of the ellipse and blows into its open end.

Windspeed 23 to 37 knots (11.8 to 18.0 m/sec), upper range: rows.—In the upper speed range of this category the pattern assumes the appearance of parallel rows of cloud elements. These rows may or may not be continuous over large distances. The wind direction parallels the orientation of the rows, but there is an ambiguity of 180°. This technique is subjective and, because of the small scale of these cloud patterns in the Tiros photographs, experience is required to gain skill in its use.

Satellite pictures of mountain lee waves, such as that shown in figure 16, have been used to estimate the average windspeed in the troposphere (ref. 20). In this study the distance across a group of well-defined waves in the photographs was measured. The wavelength was taken to be the measured distance divided by the number of waves in the interval. It is estimated that this average wavelength can be determined to within about 1.6 kilometer. The average windspeed between 85 000 and 20 000 N/m² was computed for each of the four cases in the study. Each case came from different areas, as follows: the Andes Mountains in South America, the Sierra Madre Occidental Mountains in Mexico, the Cascade Mountain Range in western United States, and
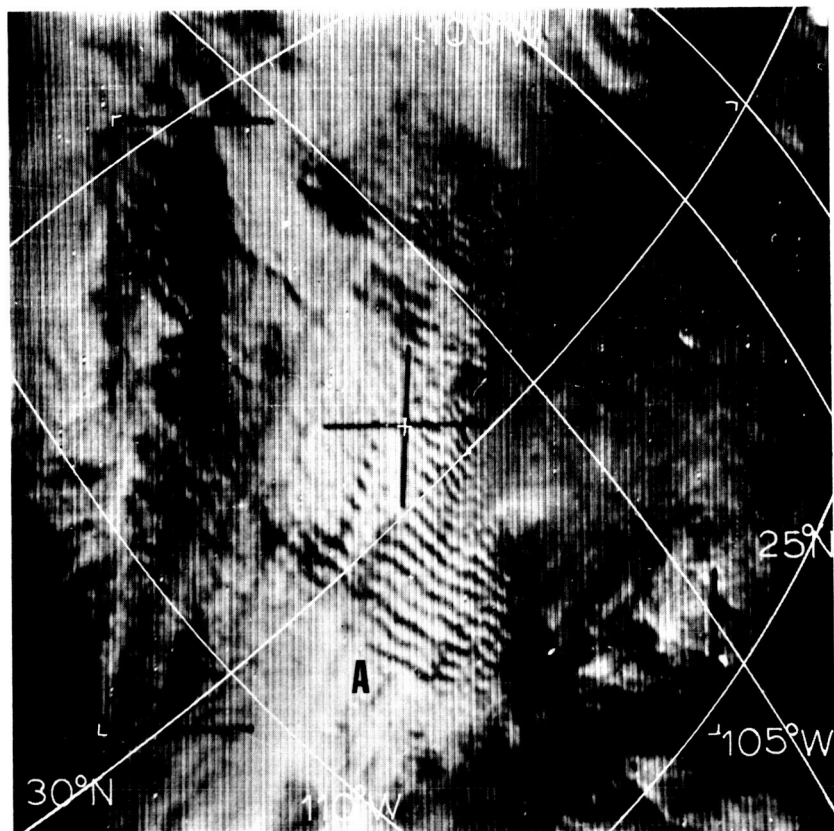
Figure 16.—Mountain lee waves photographed in the lee of the Sierra
Madre Occidental Mountains in Mexico. A latitude and longitude
grid has been superimposed on the picture. The letter A showing
the position of the center of the Sierra Madre chain has also been
added. The wavelength near the center cross-mark is about 21 kilo-
meters.

the Appalachian Mountains in eastern United States. Each combina-
tion of wavelength and mean windspeed was compared with a relation-
ship developed by Corby (ref. 21) and agreed quite well, except for the
case of the Appalachian Mountains. The relationship depends upon
the condition that the mean stability of the troposphere remains rela-
tively constant with time and from place to place. The stability in the
Appalachian area was compared with that in the other areas and found
to be substantially less.

Thus, it may be valid to measure the wavelength of mountain lee
waves and from that estimate the average windspeed in the troposphere

using Corby's empirical relation, although the relation may have to be modified somewhat to permit differences in stability. However, the introduction of a thermal stability parameter is a plausible hypothesis to explain the discrepancy in this one case. Further tests of this hypothesis are needed.

Cloud and terrestrial albedo.—In the preparation of guides for cloud interpretation from satellite pictures, the picture image is often described in terms of pattern, structure, dimensions of the patterns and forms, and brightness. However, brightness has been specified subjectively in terms of a number of gray scales. A quantitative scale would provide a more objective basis and is desirable for improved interpretations, for digital manipulation of the pictures, and for studies of the physical characteristics of clouds. One approach is to compute the radiance and albedo from the satellite pictures. Reference 22 describes a procedure for this involving the computation of radiance from film density and correcting this radiance for a number of system and atmospheric effects such as shutter speed, nonuniformity of film, warm-up effect, image persistence, solar elevation, viewing angle, multiple scattering in a Rayleigh atmosphere, and ozone in the atmosphere.

Tiros VII pictures were obtained for five separate orbits, and albedos were computed for some 86 points, of which about two-thirds were cloud surfaces and the remainder were water, land, or snow surfaces. Each point was read as many times as it appeared in the photographs. This generally ranged from 5 to 10 points. A summary of the albedos determined from the photographs is given in table I (ref. 22), where n represents the number of reflecting points measured in the corresponding category, with each point being measured, on the average, in five consecutive pictures. The table shows the albedo varying from 92 to 86 percent with changes in the size of the cumulonimbus cloud. Frontal-type clouds composed of cirrostratus and layers of middle and low clouds which yielded light precipitation were found to have an average albedo of 74 percent. Albedos of 32 and 36 percent were found for typical cirrostratus and cirrus. These values seem to be just above the threshold of transparency to objects of high contrast at the ground, such as a coastline separating semiarid land and the sea. In one case of cirrus associated with the jetstream, a value of 25 percent was determined, which may be compared with 18 percent found for the nearby land.

Clouds followed by the letters "MCO" represent "mostly cloud covered" according to Meteorological Satellite Laboratory nomenclature, or 50 to 80 percent cover. The table shows that stratocumulus MCO over land is slightly more reflective than stratocumulus masses within an extensive cloud sheet over the ocean, suggesting a greater ground than water contribution. Cumulus of fair weather MCO over

Table I.—*Average Albedos in Percent Determined by Satellite for Various Cloud and Terrestrial Surfaces*

[From ref. 22]

Surface	n^1	Albedo, percent
Cumulonimbus:		
Large and thick	8	92
Small, top estimated 6 km	1	86
Cirrostratus: Thick with lower clouds and precipitation	7	74
Cirrostratus alone, over land	1	32
Cirrus alone, over land	2	36
Stratus:		
Thick, approximately 0.5 km, over ocean	14	64
Thin, over ocean	2	42
Stratocumulus masses within cloud sheet over ocean	4	60
Stratocumulus: MCO, over land	3	68
Cumulus and stratocumulus: MCO, over land	4	69
Cumulus of fair weather: MCO, over land	2	29
Mostly snow-covered mountains above timber, 3-7 days old	3	59
Sand:		
White Sands, N. Mex.	1	60
Valleys, plains, and slopes	5	27
Sand and brushwood	2	17
Coniferous forest	4	12
Great Salt Lake	2	9
Ocean:		
Pacific	2	7
Gulf of Mexico	6	9
Gulf of Mexico—sunglint	3	17

[1] n is the number of reflecting points used in each category, each point measured, on the average, in five consecutive pictures.

land, verified from ground observations but shown only by a smooth gray tone in the satellite picture, yields an albedo of 29 percent when integrated with the albedo of the ground and shadows below, which is known to be about 15 percent.

Other measurements, not tabulated here, revealed a decrease in albedo from 70 to 51 percent for a nearly complete snow cover 3 and 7 days old, respectively. The snow fell on rough, mountainous terrain above the treeline and totaled several inches. The 4-day change is considered quite representative, since the nearby coniferous forest in Yosemite, Calif., only changed from 12 to 14 percent over the same time interval. Also of interest is the albedo of 60 percent found for White Sands, N. Mex., with a solar elevation of 78° and nadirs of 17° to 28°. This value may be compared with the 63 percent measured by Coulson

(1964, personal communication) in the laboratory on a sample of gyp-
sum from White Sands under identical light source and nadir-angle
conditions.

Another series of albedos for the Mojave Desert, not tabulated here,
averaged 39 percent with a solar elevation of 57°.

After refinements and corrections were applied to the readings, it was
found that the standard deviation of a series of readings, from suc-
cessive pictures, on the same reflecting surface averaged about 15
percent of the radiance. A comparison of the albedos measured by the
satellite with those given in the literature shows that the satellite
values are high by about 10 percent. However, albedos for thick cloud
layers topped by ice crystals were not found in the literature. These
higher-than-expected values may have been caused by changes in the
vidicon system after launch or possibly by added specular reflection
from the ice-crystal-topped clouds.

Satellite Radiometric Measurements

Introduction

Radiometric measurements in the visible and infrared have been
made intermittently since 1960 by Tiros II, III, IV, and VII. Measure-
ments of reflected solar radiation have been acquired within filtered
passbands of approximately 0.2 to 6 μ and 0.55 to 0.75 μ, and of emitted
long-wave radiation within passbands of approximately 8 to 12 μ,
8 to 30 μ, 6 to 6.5 μ, and 14.8 to 15.5 μ. Tiros VII has acquired con-
tinuous radiometric data over the Earth for almost 2 years, increasing
significantly the potential of its data for use in climatological applica-
tions.

Table II lists the nominal wavelength intervals of the Tiros radi-
ometers and the approximate months of usable data (ref. 23).

Tiros MRIR Measurement

Analysis of Radiation Data.—No significant changes have been
reported during 1965 concerning the total emitted long-wave radiation
or the albedo of the Earth based on Tiros radiometer measurements.
Results prior to 1965 are given in the section on "Satellite Radiometric
Measurements" in reference 1 (p. 59). The operation of the Tiros
VII radiometer, seasonal and annual values of the long- and short-wave
radiation based on Tiros VII data, and radiation measurements (8 to
12 μ) and some diabatic properties of the atmosphere are discussed.

Coverage.—The nearly circular orbit of Tiros VII is inclined to the
equator at 58° and has a mean height of 635 kilometers. For this
reason the polar regions cannot be observed. For data to be accepted,
the maximum allowable angle of the sensor optical axis from the nadir

Table II.—*Nominal Wavelength Intervals of Tiros Radiometers*

Nominal wavelength interval	Tiros II	Tiros III	Tiros IV [1]	Tiros VII
6–6.5 μ (H$_2$O absorption).........	X (1)[2]	X (1)	X (5)	....
8–12 μ (atmospheric window).......	X (5)	X (2)	X (5)	X (24)
8–30 μ (long-wave radiation).......	X (1)	X (1)	....	X (24)
14.8–15.5 μ (CO$_2$ absorption)......	....	....	....	X (24)
0.2–6 μ (reflected solar radiation)....	X (0)	X (2)	X (5)	X (24)
0.55–0.75μ (reflected solar radiation in visible).....................	X (0)	X (1)	X (5)	X (24)

[1] Only 4 channels were used on Tiros IV.

[2] The X's indicate the channels included on each satellite radiometer and the parenthetical numbers indicate the approximate number of months of usable data.

was 45°. Therefore, the coverage was extended beyond the subsatellite track to latitudes 63.5° north and south. For our purposes, this broad coverage which includes 89.5 percent of the world's surface area is called "quasi-global." However, data gaps exist within these latitudes because of blind orbits. There is a temporal coverage problem because of the orbital regression and the motion of the Sun. A period of 76 days (the "orbital synodic cycle") is required for the orbital nodes to move through one complete cycle relative to the Sun, and hence for all latitudes to be sampled at all local times. One item of note is the poor albedo sampling relative to long-wave data due to the lack of coverage and the solar contamination of the sensor.

Ideally, the best inference of total long-wave radiation should derive from measurements in the 8- to 30-μ channel and the best inference of total reflected solar radiation should derive from measurements in the 0.2- to 6-μ channel. However, because of engineering problems and the long-term stability of the sensors, the 8- to 12-μ and 0.55- to 0.75-μ channels were used.

The raw data were corrected for the observed degradation in the instrumental response and an empirical correction of total flux was made as a first approximation for the observed limb effects compared with the theoretically determined limb darkening. Also, the albedo data were adjusted to yield radiative equilibrium . The values of the outgoing long-wave radiation are summarized in table III.

8- to 12-μ Radiation Measurements and Some Diabatic Properties of the Atmosphere.—Medium-resolution satellite radiation measurements

Table III.—*Final Seasonal and Annual Values of Long- and Short-Wave Radiation*

Season, months	Planetary long-wave radiant power, 10^{15} cal/min	Solar radiation, 10^{15} cal/min		Planetary albedo, percent
		Reflected	Incident on planet	
J–J–A............	1725	699	2457	28.4
S–O–N............	1725	922	2574	35.8
D–J–F............	1712	859	2609	32.9
M–A–M..........	1746	796	2544	31.3
Annual........	1727.3	819.4	2546.7	32.2

have shown the applicability of satellite data for assessing relative diabatic heating and cooling in the atmosphere on a scale about half the wavelength of the smallest "synoptic" eddies (ref. 24). The variations in the 8- to 12-μ radiation temperatures are well related to the variations in the outgoing long-wave flux and, to a lesser extent, to the effective cloudiness. The relationship between the 8- to 12-μ effective blackbody temperature and the *total* radiative flux divergence (long wave and short wave) is better than the relationship between the 8- to 12-μ effective blackbody temperatures and the long-wave flux divergence. These temperatures are correlated with the latent heating component in the same sense as they are with the radiative diabatic component, but are correlated in the opposite sense with the boundary heat flux. It also appears that the effective blackbody temperature in its tabulated form may be related to the total diabatic cooling within the atmosphere; objective cloud information and additional radiometric observations may assist in the establishment of quantitative relationships.

Further empirical studies are needed for climatic regions and seasons to establish the feasibility of specifying the distribution of atmospheric diabatic heating from satellite measurements and numerical computations.

Nimbus HRIR Measurements.—The HRIR scanning radiometer was orbited for the first time on Nimbus I to map nighttime cloud cover, and cloud-top and surface temperatures. The radiometer scans the Earth at right angles to the orbit track with an instantaneous field of view of 0.5°, which corresponds to a subsatellite ground resolution of 6 kilometers (3¼ nautical miles) at an altitude of 750 kilometers (about 400 nautical miles). Its single sensor, a lead selenide photoconductor detector, is radiation cooled to −75° C, and operates in the 3.4- to 4.2-μ "window" (ref. 25).

The area measured during one mirror scan forms a band perpendicular to the orbital path which was widest at the horizons, and narrowest at the subsatellite point. Approximately 2300 adjacent bands covered one nighttime orbit. Pictorial strip records cover a region from the North to the South Poles on the nighttime side of the Earth (ref. 26).

As a prelude to illustrating the successful HRIR technique for providing a picture of the Earth and its clouds as seen in the infrared, it is instructive to review the physics of this process. The intensity of radiation being measured from the ground and cloud tops is a function of the temperature of the radiating surfaces. The scheme devised to apply the data to operational purposes was to convert different intensities of radiation into a gray scale so that the higher levels of radiation emitted by surfaces of higher temperatures (e.g., the surface of the Earth) would appear dark, and the lower levels of radiation coming from surfaces with lower temperatures (e.g., cloud-top regions) would appear lighter. In this manner, the clouds would appear white over a darker background. Moreover, colder clouds extending to higher altitudes would appear whiter than lower clouds having warmer tops. This is illustrated in figure 17 which is a small section of an HRIR orbital swath. The upper half of the illustration shows Hurricane Gladys as it is pictorially reconstructed from the HRIR measurements such as are shown in the lower half of the illustration. This is a single analog trace of an east-west scan path of the radiometer through the hurricane. It required many such scans to reproduce the entire picture. The trace indicates the temperature of the cloud top. The horizon-to-horizon length of the scan is about 4800 kilometers. It appears from the temperature analysis that the radiometer was able to detect all the way down to the sea surface in the eye of the hurricane. The latter is the high, central "spike" on the trace. Significantly, the temperatures can be read from the original trace to within 1° Kelvin. This degree of temperature sensitivity demonstrates a tremendously useful tool for cloud-height analysis. It further shows that 100 temperature gradations can be derived from the radiation traces (ref. 27).

The HRIR has had outstanding success in providing continuous nighttime coverage of clouds with pictorial presentations comparable in quality to Tiros television pictures. Temperature resolution was lost during daytime hours, mainly because the reflected solar radiations mask the telluric emission. It has been determined, since the Nimbus I flight, that the HRIR data have a variety of uses, such as the measurement of cloud height and sea-surface temperature, and the observation of ice formations, terrain features, and soil moisture (ref. 26).

Detailed studies of Nimbus I data have disclosed a wide geographical
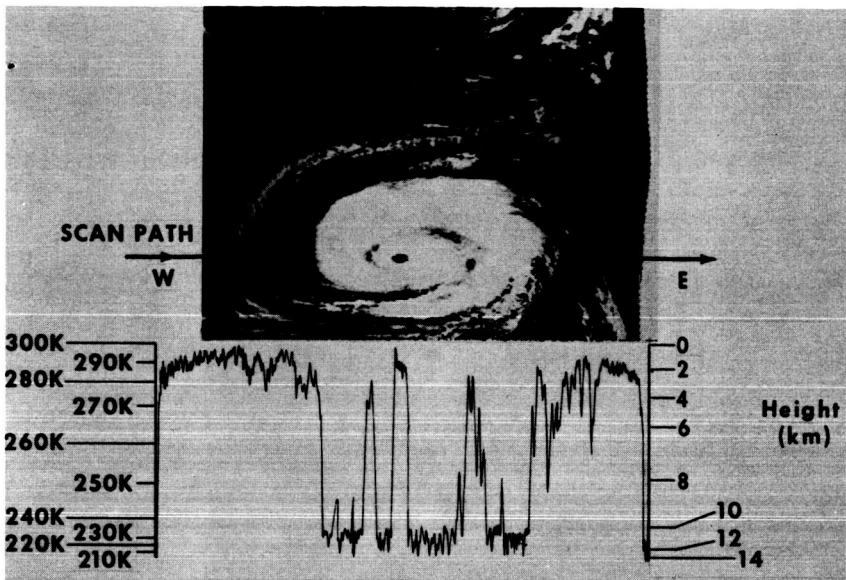
Figure 17.—Analog trace of single scan through Hurricane Gladys
(September 18, 1964; 0422 U.T.)

coverage of useful cloud-system and ice-survey information. For example, nighttime HRIR observations can be useful in detecting cloud systems as far south as the Antarctic Continent. This would be especially useful in the winter months, when the more extended darkness would permit longer periods suitable for HRIR observations. This is the season when conventional data are even more sparse than during the summer. The HRIR could also be used for ice surveys, as shown by the ice-free areas and "breaks" that are visible. With further study, the HRIR observations may provide additional clues useful in predicting cyclone movement in the Antarctic area (ref. 28).

The Nimbus I HRIR mapped the cloud cover and terrestrial features by measuring their radiating temperatures at night—when there is no solar interference—through an atmospheric window between the 4.26-μ absorption band of carbon dioxide and the 3.17-μ band of water vapor. Because this is a window region, a large fraction of the radiation measured by the radiometer originates from underlying cloud or ground surfaces. For a perfectly clean window region—where there is no atmospheric absorption—all of the measured radiation originates from the surface, and the surface radiating temperature is therefore measured directly. At the other extreme, in a highly absorbing region, all of the surface radiation is absorbed by the atmosphere and, in this case,

satellite measurements would not give any indication of the surface radiating temperature. In the range between a perfectly clean window region and a highly absorbing region, the HRIR window region falls very near the perfectly clean window extreme.

It has been determined quantitatively that the overlying atmosphere has little effect on the outgoing radiation observed by the HRIR and that the HRIR measurements, therefore, give a good estimate of the surface temperature (ref. 29).

Thus, a variety of different geophysical and atmospheric facts can be inferred from the observation of temperature variations over the Earth's surface. Over heavily vegetated regions of the Tropics, the ground temperature can be measured. Because of the larger heat capacity of this type of terrain, its effect on air temperatures is similar to that of oceans; the ground acts as a reservoir which heats or cools the air moving over it, depending on its temperature. At higher altitudes, especially over dry sandy terrain, the heat capacity of the ground is so small that near midnight, when solar radiation is absent, the satellite-measured ground temperature is much less than the air temperature, demonstrating temperature inversions. Over more solid rock surfaces, the satellite-measured ground temperatures are more nearly equal to the air temperatures. Contrasts in the thermal properties of the surfaces usually exhibit a very pronounced fine structure in the satellite observations. In many cases, these contrasts can be interpreted, qualitatively at least, as a measure of moisture content of the ground, changes in the vegetation, or in the geological formation along the ground (ref. 30).

Operational Applications

During 1965 satellite cloud pictures have been incorporated into the regular daily weather analyses and forecasts of the Weather Bureau. Subsequent to the launch of Tiros IX in January 1965, cloud data provided by Tiros VII, VIII, IX, and X have been used to prepare daily global cloud maps for use in operational weather forecasting. Each day approximately 450 cloud photographs are used to prepare 20 to 25 cloud analyses.

Storm Tracking and Identification

Cloud pictures continue to be used in data-sparse areas on an equal basis with the conventional observations, and often as the primary basis for the weather analysis, but integrated to achieve an analysis compatible with data from all sources.

Since the advent of daily global cloud maps, the ability to locate and accurately track cloud systems has been enhanced. The satellite

cloud information is being used in conjunction with other observations to prepare weather analyses considerably more accurate than those based solely on continuity.

Tropical Analysis

Cloud pictures provided by Tiros IX and X have been used extensively in tropical weather analyses and forecasting. Table IV shows the tropical storms, hurricanes, and typhoons observed and tracked in 1965 by the Tiros satellites. A study of cloud formations during the buildup of cyclones showed a definite correlation between pressure and cloud formations. Figure 18 shows that once the pressure of a storm
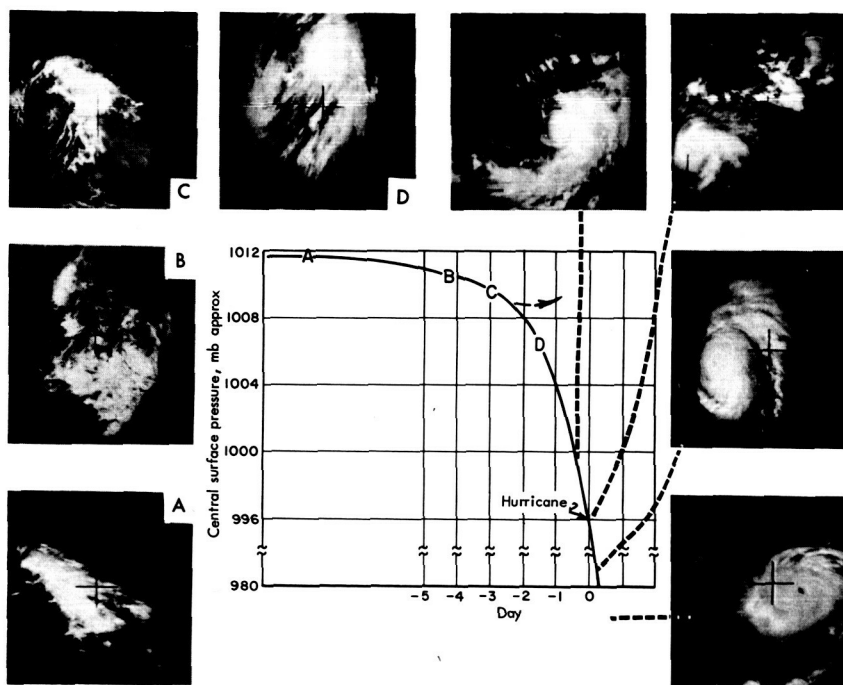
Figure 18.—Cloud development in tropical cyclones as seen by Tiros.

drops below a critical pressure, indicated at the knee of the curve, there is a high probability that a full-scale cyclone or hurricane will develop. The continuous surveillance of storm areas by satellites combined with this empirical study will, it is hoped, provide a method of forecasting the development of hurricanes.

Special Storm Advisories.—Over 500 000 Tiros cloud pictures have been used by the Weather Bureau in the preparation of approximately 22 000 cloud analyses which have been used for daily weather analyses

Table IV.—*Tropical Storms Observed by Tiros Satellites. January 1965 Through December 1965*

[*Indicates storm discovered by satellite observation]

Atlantic Ocean	Eastern Pacific Ocean	Western Pacific Ocean	Indian Ocean
Hurricane Anna, 8/65	Tropical storm Victoria, 6/65	Typhoon Patsy, 1/65	Tropical low Rose, 4/65
Hurricane Betsy, 8/65	Tropical storm Wallie, 6/65	Tropical storm Ruth, 1/65	
Hurricane Carol, 9/65	Tropical storm Ava, 6/65	Typhoon Amy, 5/65	
Tropical storm Debbie, 9/65	Tropical storm Bernice, 6/65	Typhoon Babe, 6/65	
Hurricane Elena, 10/65	Tropical storm Claudia, 8/65	Typhoon Carla, 6/65	
	*Tropical storm Doreen, 8/65	Typhoon Dinah, 6/65	
	Hurricane Emily, 8/65	Tropical storm Emma, 6/65	
	Tropical storm Florence, 9/65	Typhoon Freda, 7/65	
	Tropical storm Glenda, 9/65	Tropical storm Gilda, 7/65	
	Tropical storm Hazel, 9/65	Typhoon Harriet, 7/65	
		Typhoon Ivy, 7/65	
		Typhoon Jean, 7/65	
		Typhoon Lucy, 8/65	
		*Typhoon Mary, 8/65	
		Typhoon Olive, 8/65	
		Typhoon Rose, 9/65	
		Typhoon Shirley, 9/65	
		Typhoon Trix, 9/65	
		Tropical storm Virginia, 9/65	
		Tropical storm Wendy, 9/65	
		Tropical storm Agnes, 9/65	
		Typhoon Bess, 9/65	
		Typhoon Carmen, 10/65	
		Typhoon Della, 10/65	

and forecasting purposes. Over 2600 special storm advisories have been issued by the Weather Bureau (ESSA) on the basis of these satellite data.

Nonmeteorological Applications

The technical requirements for meteorological satellite sensors (e.g., coverage, resolution, sensitivity, spectral response) are such that the data obtained can be interpreted not only in terms of physical atmospheric processes but also in terms of many other geophysical parameters. For example, cloud-cover pictures also show large areas of water, land, vegetation, snow, and ice. The broad range of scientific, economic, and operational applications of these data were described in reference 1.

Ice

Coordinated with the launch of Nimbus I, the Canadian Government sponsored Project Nairec (*Nimbus Arctic Ice Reconnaissance*) to use the data obtained from the Nimbus APT system (ref. 31). The objective of the project was to receive and reproduce the pictures in "real time," and to learn something of how such pictorial information could be used in an Arctic ice forecast system. In 15 days, 130 APT pictures were received at Frobisher Bay, Northwest Territories, of which 76 were received as whole pictures. Figure 19 shows the positions over which the pictures were taken. This represents an average of more than eight pictures per day, or nearly three per usable orbit. The pictures obtained at Frobisher Bay possessed better resolution than had been expected. Geographical detail and cloud configurations are well defined. Using proper interpretation techniques, the pictures were quite suitable for the extraction of ice information.

Because of the season and limitations on the northernmost positions at which Nimbus I took APT pictures, only three photographs were obtained in which sea ice was discernible. (A request to the Nimbus I project to extend these limitations could not be acted on before Nimbus I ceased operation.) The small quantities of ice seen in these three pictures showed general agreement with the ice information available, but no detailed comparisons were possible. Experience gained from earlier work using Tiros data and the appearance of ice caps and various snow-covered mountains and islands in the Nimbus pictures led the authors to the conclusion that had ice been present in significant quantities, it would have been identified and mapped. Further data utilization for ice mapping is discussed below.
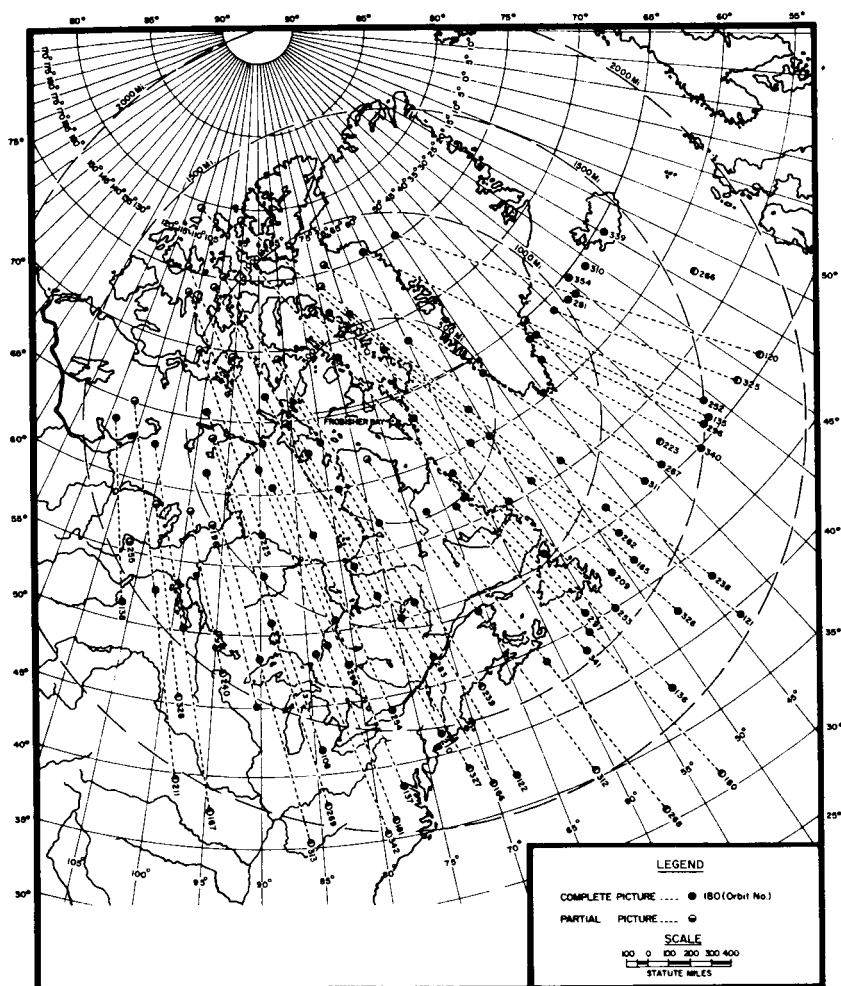
Figure 19.—Nimbus I APT coverage at Frobisher Bay, Northwest Territories, Canada, September 2 to September 21, 1964.

Cartographic and Geological Uses of the Data

The Geological Survey of the U.S. Department of the Interior has put the improved TV pictures from the Nimbus AVCS to uses which resulted in cartographic changes to be incorporated in the revision of their 1:10 000 000 Antarctic plastic relief model. Three of the more significant changes are listed below and shown in figure 20.

(1) Mount Siple was repositioned 2° west from the position given on existing maps. This is a 10 000-foot (3000-meter) mountain, on the coast, often used as a location or orientation point.
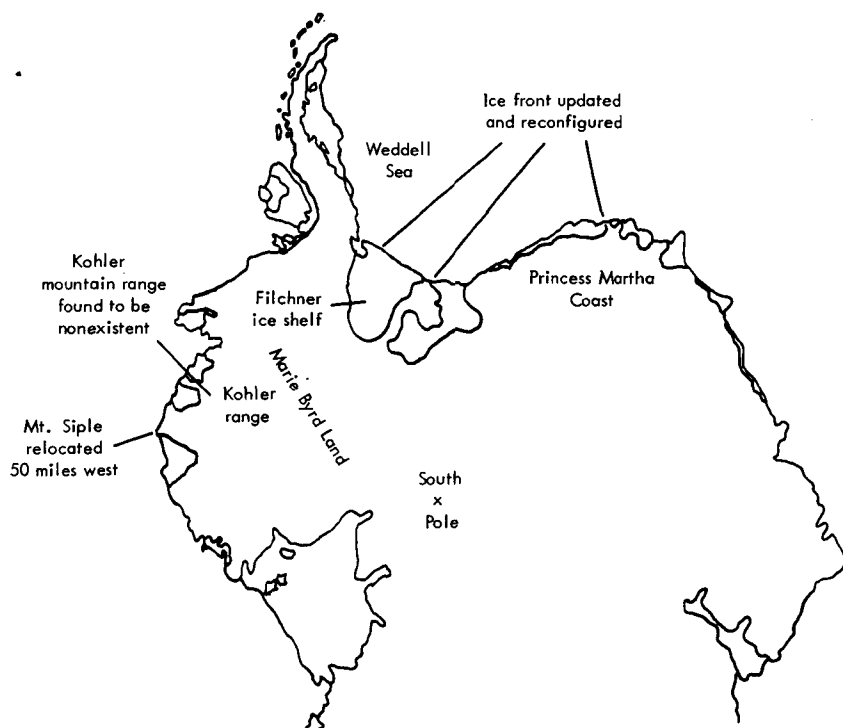
Figure 20.—Geological Survey use of Nimbus I AVCS pictures.

(2) A mountain group in the Kohler Range area was eliminated. (This group evidently was sighted by two different expeditions and subsequently positioned by them in two different locations. Antarctic maps currently show two mountain groups in this area, whereas Nimbus I photography indicates that there is only one group.)

(3) The ice-front information was updated and the ice front itself reconfigured in the Filchner ice shelf, Weddell Sea, and Princess Martha Coast areas. (The above information is from a private communication from the Acting Chief Topographic Engineer to the Nimbus Project Manager, dated September 15, 1965.)

While observing the remarkable geographical relocations in the Antarctic region, some other interesting AVCS disclosures in the same area also come to light. First, the formation of a large Antarctic tabular iceberg located at the junction of the Palmer Peninsula and the Filchner ice shelf is shown in figure 21.

As another example of AVCS use, C. I. Taggart, a noted Canadian photointerpreter, was able to determine in figure 22 (taken of islands
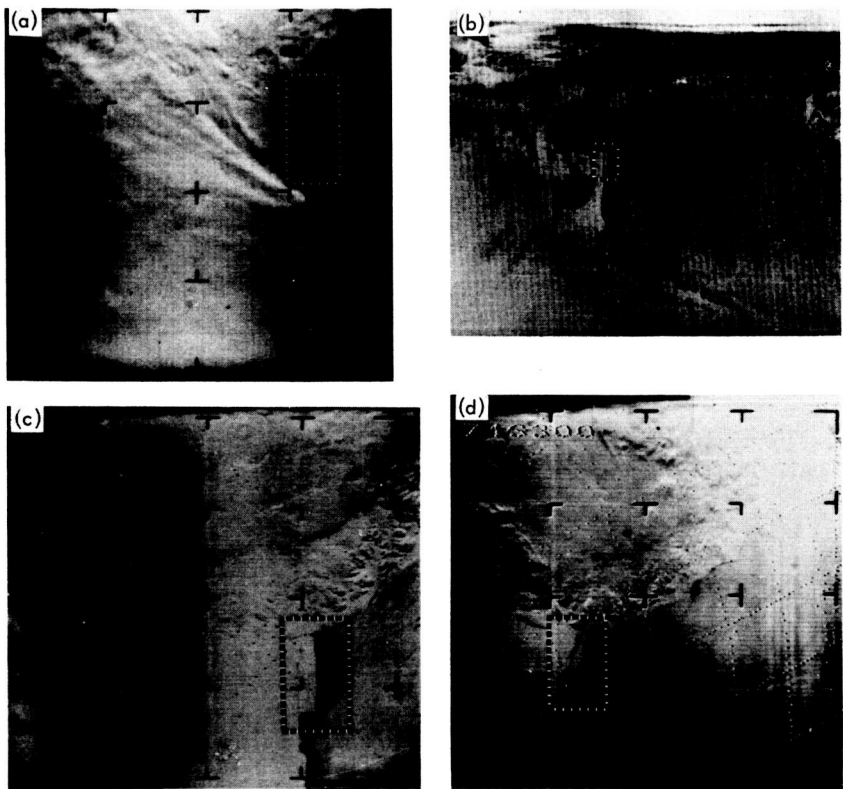
Figure 21.—Nimbus I pictures of a tabular iceberg on the east coast of
Antarctica. (*a*) September 8, 1964:   pass 168 r/o 167, 1834Z, camera
2. (*b*) September 16, 1964:   pass 291 r/o 288, HRIR. (*c*) September
16, 1964:   pass 285 r/o 284, 1831Z, camera 2. (*d*) September 16,
1964:   pass 286 r/o 285, 2008Z, camera 3.

in the James Bay on September 6, 1964) that extensive underwater
shoals exist around the semicircular island shown (Akimiski Island).
The light area is the shoal surface.

As another AVCS example, figure 23, which was taken of the Paris
Basin on September 13, 1964, discloses exposed Upper Cretaceous chalk
formation of the Barren Champagne.   This is a relatively light area to
the right of fiducial crossmark at the center of the picture.   The black
band to the immediate right of the Barren Champagne represents the
black lacustrine sands and clays of the Lower Cretaceous called the
Humid Champagne.   Several visible rivers cut through the Barren
Champagne.
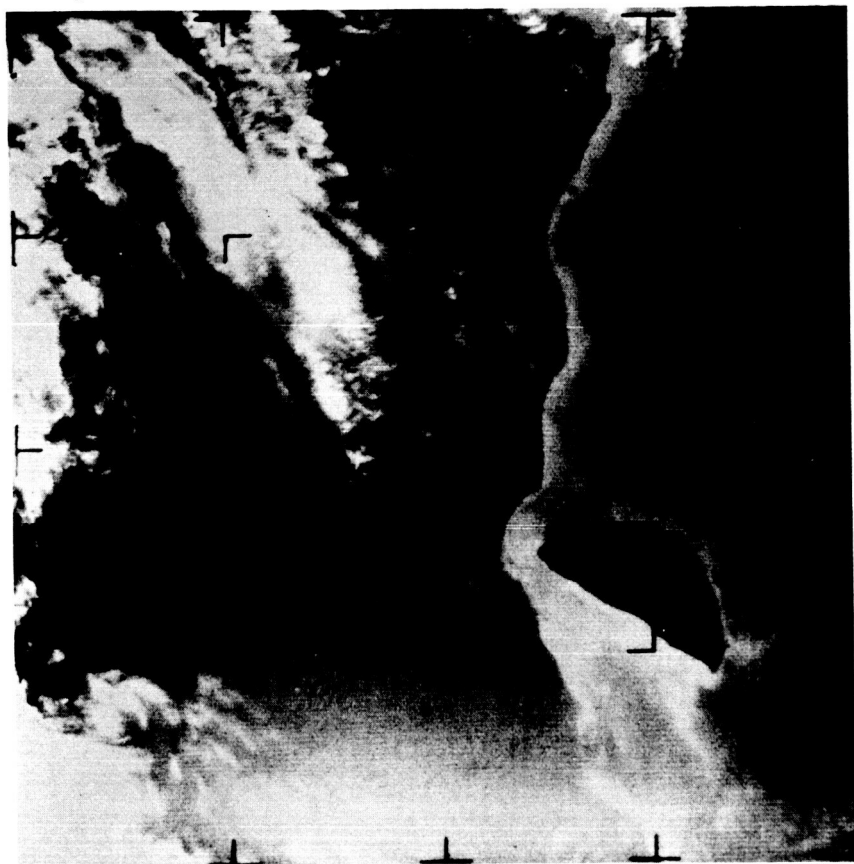
Figure 22.—Nimbus I AVCS picture of islands in James Bay.

Further use of the Nimbus I APT data in interpretation of geological features was reported in reference 32. During an examination of Nimbus I photographs, a photograph exposed from 493 kilometers above Lake Ontario (orbit 254, September 14, 1964) clearly showed the complex folded pattern of the Appalachian Mountains in the Pennsylvania region.

Detailed examination of the photographic pattern as to size, shape, and tone of these Appalachian features showed close correlation with the rock-type units as depicted by the 1:250 000 Geologic Map of Pennsylvania, published by the State Geological Survey in 1960. Variations in tonal pattern agreed in fine detail with the rock groups. The boundaries of each distinctive group were clearly delineated on the photograph.
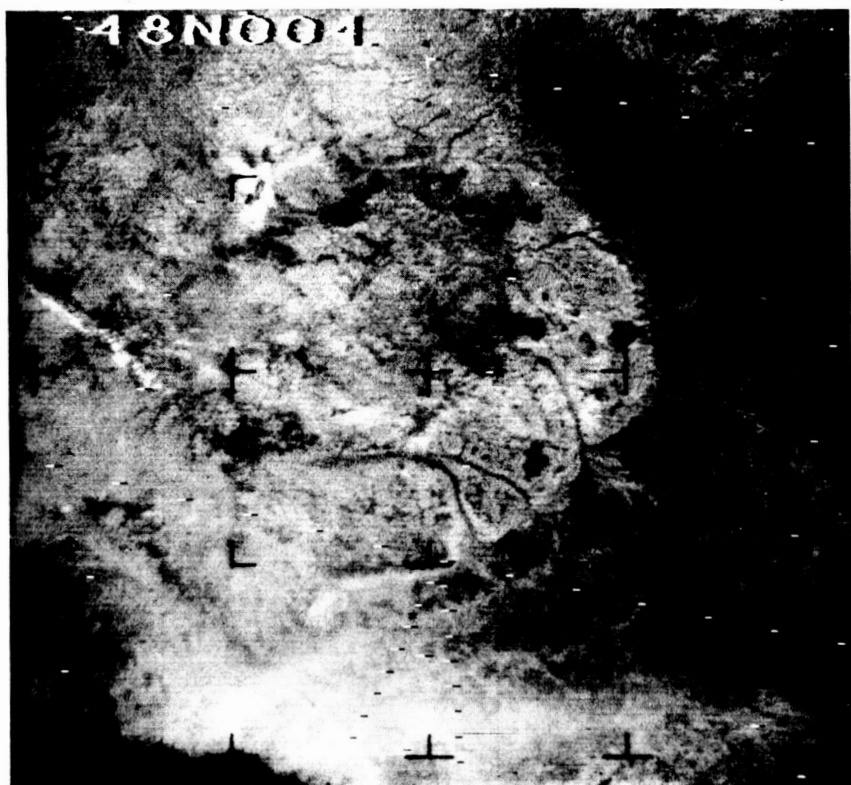
Figure 23.—Nimbus I AVCS picture of the Paris Basin.

The tonal variations can be linked to the forest cover, and forest boundaries are also known to mark changes in geological formations, particularly as is evidenced to the northeast in the Adirondack Mountain area.   However, in the Pennsylvania area, forest cover alone is not sufficient to account for the very distinct and uninterrupted sizes and shapes of the tonal pattern that relate to the rock-group areas.   Large portions of these individual group areas are known to be under intense varying cultivation, with other areas of considerable magnitude given over to industrial complexes and large urban developments.   These, of course, influence, but do not upset or disrupt, the shapes, sizes, or tones of the geological patterns seen on the satellite photograph.

The particular photograph is not a peculiar freak of lighting; camera position, etc., for the same features are also reproduced in an earlier Nimbus I APT picture (orbit 137, September 6, 1964).   In this earlier picture, the same features appear in similar shapes, sizes, and tones as on the photograph taken 8 days later.

It is therefore felt that the variations of tones shown in this study are specifically related to the rock types of a detailed geological map, and are greatly influenced by the different reflectivities of the various rock and soil textures. Further, it would appear that these textures have a greater influence on the tonal qualities in a very-high-altitude photograph than when the pattern is cluttered with identifiable and directly visible features such as vegetation and industrialization as is the case with conventional aerial photography.

Sea-Surface Temperatures

As outlined in reference 1, sea-surface temperatures are important to meteorology as well as to oceanography and in support of military requirements and commercial activities, such as fishing and shipping. All of these applications are severely hampered by the lack of adequate sea-surface-temperature information. During 1965 a study, based on infrared data, was made of the feasibility of observing sea-surface temperatures or temperature gradients from a satellite (ref. 33). The following conclusions were reached:

(1) A satellite can measure patterns of sea-surface temperature where cloud cover does not interfere. This has been borne out, in part, by the consistency of IR data for areas of known sea-surface-temperature persistence, which has given some indication of the validity of the observed sea-surface-temperature patterns on single passes.

(2) The consistency tests have revealed that large-scale patterns are easily recognizable and change little from day to day. Persistent small-scale patterns can also be detected on repeated passes.

(3) At least one conventional sea-surface-temperature measurement is required to serve as a benchmark if good absolute values are required. (This is a result of uncertainties in atmospheric attenuation of infrared radiation and in sensor calibration and degradation for the Tiros radiometer.)

(4) In daytime, Tiros channel 5 data, converted to an albedo, are suitable for detecting cloud-contaminated points.

(5) No method for reliable cloud detection at night is presently apparent.

(6) Other sources of cloud-cover information, that is, conventional meteorological observations and satellite TV data, are insufficient for determining all of the significant, clear areas for satellite observation of sea-surface temperature. That is, the data are inadequate in many areas to determine whether or not the sky is clear enough so that sea-surface temperatures can be measured.

(7) Comprehensive studies or operational analyses of sea-surface temperature will require the processing of large quantities of satellite radiation data. The application of these techniques to satellite IR data can significantly increase our knowledge of sea-surface temperature and its patterns, gradients, and variations over several scales of time and space at which they have significant scientific and practical applications.

UPPER ATMOSPHERE (ABOVE 30 KM) METEOROLOGICAL SOUNDING ROCKETS

Background

As was shown in reference 1, data from meteorological sounding balloons indicated the necessity for data beyond the altitudes which the balloons could reach. During the International Geophysical Year (IGY), 1957–58, certain sounding-rocket experiments were conducted at the higher altitudes. These experiments added much to our knowledge of the atmosphere, but made apparent a number of additional areas for investigation:

(1) The relations and mechanisms operating between and within the various regions of the atmosphere
(2) The circulation and dynamics of the upper atmosphere
(3) The relation between the general circulation and the sudden stratospheric warmings
(4) The geographic and seasonal variations in the structure of the atmosphere
(5) The relationships between solar-energy input and the variations of the structure and circulation in the upper atmosphere

It was also found that the observed variability of the atmospheric structure, especially that of the vertical wind profile, increased the difficulty of applying the small amount of data available to the design and operation of launch vehicles for aerospace missions.

Meteorological Observational Program Above 30 Kilometers

The program continues to use two classes of rockets. The larger research sounding rockets of the Nike-Cajun or Nike-Apache class are used to obtain research data up to 100 kilometers and in the development of new measurement techniques for that region. The smaller operational development sounding rockets of the Arcas and Loki class continue to obtain data routinely up to 60 kilometers and for testing components and systems. The development work is aimed toward achieving an inexpensive meteorological rocket sounding system capable

of reliable routine launches and amenable to the requirements for range support, research, and network operations.

Research Sounding Rockets and Measurement Techniques

Four experiments which have been carried aboard the Nike-Cajun class rockets were described in reference 1. These are the sodium-vapor, acoustic-grenade, falling-sphere, and the pitot-static-tube experiments.

In addition, significant progress was made in 1965 in developing an ozonesonde which will provide a continuous measurement of the ozone content of the atmosphere during a parachute descent after ejection from the rocket. Measurements will be obtained from altitudes of about 65 kilometers down to and including the ozone peak in the vicinity of 20 kilometers. Previous ozonesondes have taken measurements only at a relatively few discrete points. The system, which has been brought to the flight-test stage of development, uses an active ozone-chemiluminescent material (rhodamine B adsorbed on fine silica gel). The luminance of the material is a function of the amount of ozone present in the gas sampled and the pressure of the gas. The luminance is measured by a photomultiplier tube. The gas from the free atmosphere is drawn across the detector disk into an evacuated chamber through a small tube which regulates the flow. The pressure differential is maintained by the increasing atmospheric pressure as the ozonesonde descends through the atmosphere. This basically simple device is attached to suitable telemetry which reports the signal from the photomultiplier tube to the ground station. Thus, the sampling system will have no moving parts, use no power, and operate continuously. Flight tests are planned during the next year.

Present Research Meteorological Sounding Rocket Program

The four methods described previously continue to be used for measuring pressure, density, temperature, and wind in the 50- to 90- kilometer region. During 1965 significant steps were taken to broaden the geographic coverage of the data obtained in the NASA program. The grenade experiment was conducted for the first time at Point Barrow, Alaska, at approximately 71° north. A memorandum of understanding was signed in 1965 with Brazil which will allow the grenade experiments to be conducted from Natal (at about 5° S). The NASA 1965 mobile launch expedition conducted meteorological experiments using the pitot-static tube from aboard the U.S.S. *Croatan* near the equator and as far as 60° south. The previous farthest southerly measurements were taken at Ascension Island, about 8° south. Where possible these

firings were, and will be, coordinated with regular firings from Wallops Station and Fort Churchill.

As indicated in table V, there has been a total of 48 successful launches of research meteorological sounding rockets in 1965. The first series of these consisted of grenade experiments launched from Point Barrow, Fort Churchill, and Wallops Island. Two purposes of the launches were to obtain three-station synoptic data during a stratospheric warming event and to obtain data at Point Barrow during the polar winter night. This work was carried out during late January and early February.

During March and April the mobile launch expedition launched the eight pitot-static-tube experiments near the 80° meridian during the trip south from the equator to about 60° S. The data were taken near the time of the autumnal equinox for the Southern Hemisphere, and hence a transition period. The locations of the firings are such that profile along a meridian was obtained.

In June, a series of four sodium-vapor and trimethylaluminum experiments were launched between sunset and sunrise to determine the existence of fine-scale temporal and spatial variations in the winds from about 70 kilometers to 110 kilometers.

In August, 11 grenade experiments were launched from Point Barrow, Alaska; Fort Churchill, Canada; and Wallops Island, Va. These experiments were designed to study the temperature conditions during the occurrence of noctilucent clouds (at Point Barrow) and to obtain synoptic data from the three stations so as to provide a coarse grid for determining the general circulation and structure at the time of the event.

In October, 12 grenades were launched synoptically in 4 sets from the same 3 stations. These launches were to provide data during the fall transition period, as the flow changes from the generally weak flow of summer to the stronger, more defined flows of winter.

Other launches were made to obtain climatological data and to obtain system test data.

Operational Development Sounding Rockets and Techniques

Because of their size, complexity, cost, and range requirements, the research rockets described in the preceding sections cannot be employed on a large scale. What is required for this type of use is an inexpensive meteorological rocket sounding system capable of reliable, routine launches and amenable to the requirements for range support, research, and network operations. The overall system development is directed toward improvement, development, and design of rocket motors and

Table V.—*Monthly and Geographical Distribution of Successful NASA Research Meteorological Sounding Rocket Launches in 1965*

[G indicates grenade; Na, sodium vapor release; P, pitot-static tube; and the number indicates the number of launches greater than one.]

Month	Type of payloads launched at—				
	Wallops Island, Va.	Fort Churchill, Canada	Point Barrow, Alaska	Ascension Island, British West Indies	Shipboard (off west coast of South America)
January.....	G	G	G	....	....
February....	2G	2G	2G	....	....
March.......	....	....	....	....	3P
April.......	....	....	....	....	5P
May........	....	....	....	2P	....
June........	4Na	....	....	....	....
July........	G	....	....	....	....
August......	3G	4G	4G	....	....
September...	....	....	....	....	....
October.....	4G	4G	4G	....	....
November...	....	P	....	....	....
December....	....	....	....	....	....

sensors, and data acquisition and reduction systems. The systems now generally employed, using the Arcas- and Loki-class rockets, carry a 1- to 5-kilogram payload to 60 kilometers.

The two basic classes of measurements in use are passive and active techniques. The passive techniques of measuring wind are chaff, parachutes, and inflatable Mylar spheres; the latter technique also provides density measurements. Active telemetry has been used thus far only for direct measurements of temperature. These techniques are more fully described in reference 1.

Present Operational Development Sounding Rocket Program

The overall system development is programed so that through the evolution of several successive systems, a small meteorological sounding rocket system with a 100-kilometer-altitude capability and including direct readout will be available by the early 1970's. To increase the number of locations which can use such a system, the falling mass hazards, such as spent motor cases, must be eliminated. This system

is intended to serve as the basic unit which, with suitable modification and conversion, will be capable of worldwide use by 1975 with few limitations on launch site and environment. The cost-reduction efforts will extend to around 1974.

The data obtained from the rockets fired in testing these developments can be used in three ways: in development work; in support of other tests or missions; and in support of the cooperative, meteorological sounding rocket network (ref. 1). Each NASA sounding rocket is scheduled so that as many of these data uses as possible can be included.

The cooperative meteorological sounding rocket network, which uses rockets of these types, is currently firing rockets at a rate of about 1000 a year. The cumulative total since 1959 is estimated at over 4500 successful upper atmospheric soundings, as of the end of 1965. During the year covered by the February 1964 to February 1965 issues of reference 34, 18 stations participated in these launches (fig. 24).

During the NASA 1965 mobile launch expedition mentioned previously, eighteen Arcas rockets with the standard temperature telemetering payload and seven Hasp-type rockets with chaff payloads were launched at locations near 80° W longitude off the west coast of South America from 5° N to 60° S latitude. The data obtained have provided the first extensive exploration of this type into the circulation of the Southern Hemisphere's upper atmosphere.

Flight tests were conducted in a number of developmental areas. One test was to define an optimum high-drag payload parachute with good stability characteristics. Low drag means that either excessive parachute size and weight must be allowed for, or high fall rates tolerated. Poor parachute stability characteristics allow excessive oscillations and gliding of the parachute to occur, which introduce errors in wind measurements. Wind-tunnel and flight tests with onboard cameras have shown that the disk-gap-band parachutes (fig. 25), developed under this effort open satisfactorily at 60 000 meters and descend stably through the altitude range of interest.

The ballistic coefficient $(W/C_D S)$ of the parachute-payload system defines the descent velocity which in turn directly influences the wind-following capabilities of the parachute. Other instrument requirements which are influenced include response characteristics of the temperature-sensing payload. Figure 26 shows the descent velocity of the parachute as a function of altitude for various values of $W/C_D S$. The current Arcas system has a ballistic coefficient of about 0.06. For releases near 90 000 meters, the figure indicates that this system has an unacceptably high descent rate, as have all other current systems. Special packaging of lightweight payloads and larger, lightweight para-
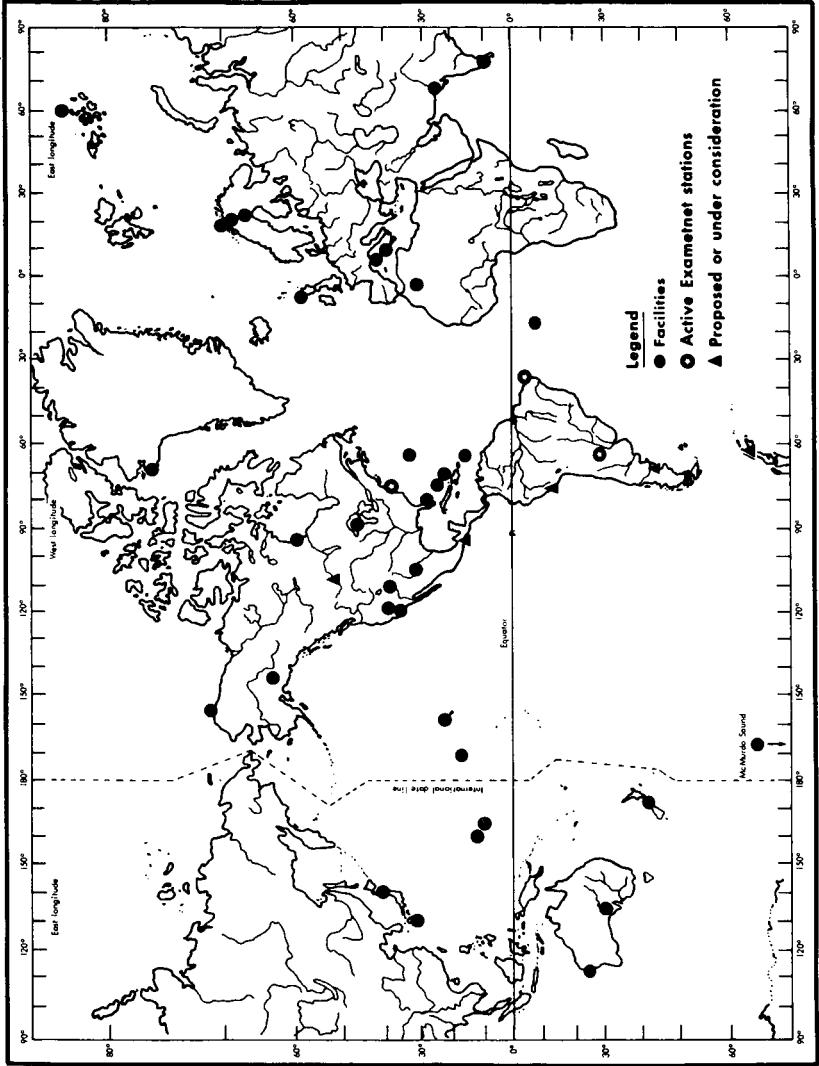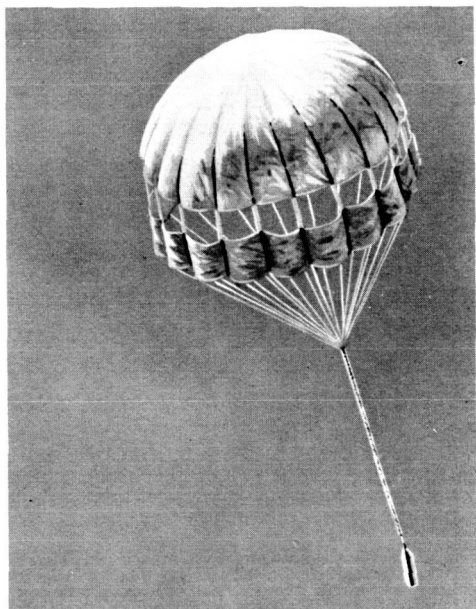
Figure 24.—Facilities for meteorological sounding rockets.

Figure 25.—Payload para-
chute test.

chutes aboard Arcas rockets have been successfully flight tested which
have $W/C_D S$ values of about 0.02, allowing either acceptable descent
rates at higher altitudes or lower descent rates (about one-half previous
descent rates) at current altitudes.

Measurements of the longitudinal accelerations, the longitudinal and
lateral vibrational characteristics, spin rate, heating rate, and internal
temperatures were obtained from Arcas rocket flights in October 1965.
The basic measurements are given in table VI.

The table shows that the linear acceleration, spin rates, and heating
rates confirm the measurements made in 1964. The vibrational levels
in the payload section of the Arcas rocket are less than anticipated and
substantially lower than payload qualification levels currently in effect.
It is believed that the information summarized in the table provides sat-
isfactory environmental data for payload design for the Arcas rocket.

The approximately 20-Hz spin rate of the Arcas rocket at separation
has caused deployment problems with parachutes and other inflatables.
"Yo-yo" despin devices have been designed to dissipate the angular
momentum and are being readied for flight test.

Complete studies of the performance of Arcas rockets have been
difficult because of incomplete knowledge of the aerodynamic char-
acteristics of the rocket system. Therefore, wind-tunnel tests are being
conducted on a $1/2$-scale model over a Mach number range of 0.6 to 4.6
and angles of attack from $-4°$ to $+20°$. Both the Arcas Robin (in-

Table VI.—*Arcas Inflight Environmental Measurements*

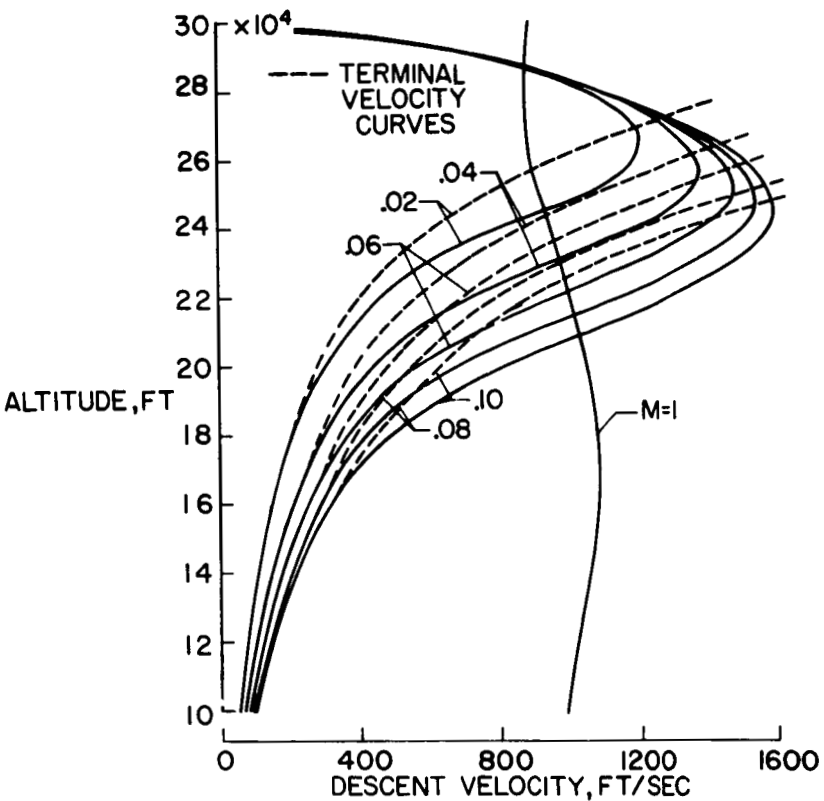|	1964 Flight	1965 Flight
Linear acceleration, g:		
Launch shock	57	64
Separation shock	74	
Steady state	3.5–4.5	3.5–5.5
Vibration; Hz, g:		
Thrust axis	....	400,0.5
Transverse	....	100,1.5
Spin rate, Hz:		
Thrusting	22	22
Separation	20	15
Heating rate, Wm²	45 400	71 500
Temperature, °C	36.7	55.5

Figure 26.—Effect of ballistic coefficient on descent velocity.

flatable sphere) and the Arcas sonde configurations become aerodynamically unstable above Mach numbers of 3 and 3.5, and large roll-and-yaw moments are inherent at large angles of attack. The slope of the C_M and C_L (pitching moment and lift) curves are definitely nonlinear and become unstable at an angle of attack of 8° or less at supersonic Mach numbers. While the stability analysis has not been completed, the trends in the evidence explain a number of inflight failures that could not be satisfactorily analyzed using available theoretical aerodynamic curves.

NASA and the Army are cooperating in a contractual effort on a technique ·to eliminate falling-mass hazards inherent in rocket-vehicle inert components. Both consumable and explosive fragmentation techniques have been demonstrated for the motor case and fins. The feasibility has been demonstrated, but significant disadvantages remain to be eliminated for both methods (e.g., weight penalties, cost, performance constraints). Further work to improve techniques is in progress.

A study was completed in 1965 outlining the type of rocket necessary to meet the long-range requirements for the system, thus forming the initial step toward developing such a system. Extension of this effort toward the final system is underway.

Results

Research Meteorological Sounding Rockets.—One of the results obtained in 1965 concerned the accuracy of the several procedures available for deriving pressure and density profiles from a measured atmospheric-temperature profile. Basically, all these procedures involve the vertical integration of the measured temperature profile to obtain the pressure profile once a reference pressure is known, either assumed or measured. Variations of the hydrostatic equation and the perfect gas law are the means by which temperature and pressure profiles can be determined from a measured density profile. However, it is concluded that while integrating measured density downward from an assumed initial temperature soon converges to an accurate temperature (or pressure, as the case may be) profile, as is done in the falling-sphere and pitot-static tube experiments, integrating a measured temperature profile yields the most accurate pressure and density results only when it is integrated upward from an initial measured pressure, as in the grenade experiment. The total error in pressure measurement by the grenade procedure is probably less than 5 percent as determined by independent observations and theoretical considerations (ref. 35).

Some of the other results of the grenade experiments are detailed in reference 36. There was good qualitative agreement between cal-

culated and observed temperature in the stratosphere at all locations, confirming the belief that the absorption of solar radiation by ozone near the 50-kilometer level provides the dominant heat source between the troposphere and the thermosphere.

It was further noted in reference 36 that in the lower mesosphere, there are practically no seasonal and latitudinal temperature variations in the altitude range of about 60 to 65 kilometers. Indeed, considering the results reported in reference 37 for Woomera, Australia (31° S), the earlier IGY data (ref. 38), and the data shown in figure 27, one may conclude that temperatures at these altitudes range generally between 230° and 240° K over the entire globe during all seasons.
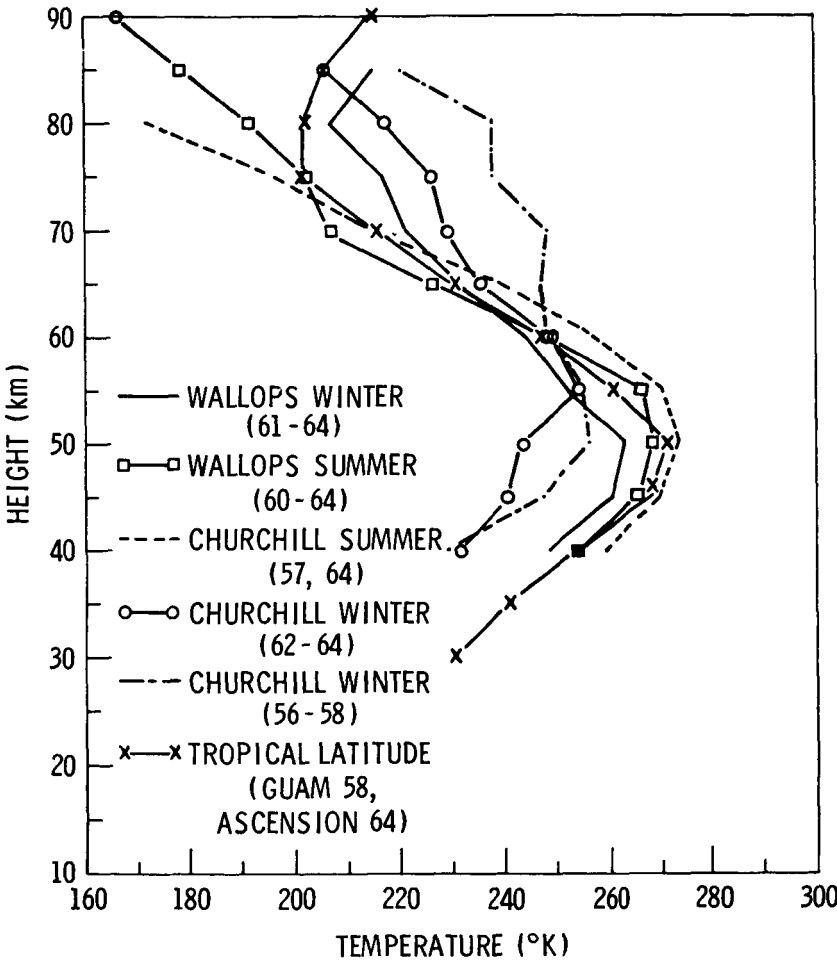

Figure 27.—Seasonal and temporal variations of the vertical temperature profile.

At equatorial latitudes, for which an average profile is shown in figure 27, there have not been sufficient soundings to deduce positively the absence of seasonal variations. However, the trend demonstrated in the observations at other latitudes, and the fact that at all altitudes the average equatorial temperature profile lies beween the summer and winter profiles observed at higher latitudes, leaves little doubt that at equatorial latitudes the seasonal variations are at a minimum.

The analysis in reference 39 of a number of the acoustic grenade soundings, supplemented by sodium releases above 70 kilometers, showed that the generally accepted circulation patterns cease to exist above about 75 kilometers. Above that altitude the circulation seems to be governed by variations with much smaller time scales than in the stratosphere and lower mesosphere. Tidal phenomena seem to be of much greater importance at those altitudes than the synoptic scale pressure variations of the lower regions.

Operational Development Sounding Rockets.—From 1958 to 1964, sounding rockets raised the height to which synoptic analyses could be made from 30 to nearly 60 kilometers.

Work in 1961 had indicated the existence of a quasi-biennial oscillation in wind between 25 and 60 kilometers. Examination of rocket-sonde wind data obtained since that time have led to several additional conclusions. The amplitude of the oscillation in the Tropics is largest near 25 kilometers and diminishes gradually above this level up to a height of 50 kilometers or more. The downward propagation noted at lower levels is characteristic of the 30- to 50-kilometer layer as well, but the phase speed is about twice as great as at the higher levels. Also brought to light by this work is the possible existence of a pronounced semiannual cycle in the zonal wind component at a height of 40 kilometers and above (ref. 40).

Other authors have used the relatively few years of data available to try to determine the worldwide character of this 26-month cycle. Their results, from reference 41, are considered preliminary because of the relatively short period for which data are available, and are summarized below.

The data indicate that the quasi-biennial west-wind maximum propagates downward at a speed of about 2 kilometers per month in tropical latitudes and about 5 kilometers per month in temperate latitudes. The oscillations at temperate and tropical latitudes appear to be in phase at heights near 25 kilometers and out of phase at heights near 60 kilometers. The amplitude maxima are near 25 kilometers in the Tropics (in agreement with ref. 40) and increase in height into the Temperate Zones.

Diurnal and semidiurnal oscillations have also been noticed, and at

one location at least, the largest amplitudes were found near 45 kilometers where the heating of the ozone by solar ultraviolet is at a maximum (ref. 42).

Another use of the wind profile data has been to evaluate temperature advection between 26 and 42 kilometers (ref. 43). The rms values of temperature advection are presented as functions of season and altitude. These values are used to infer the order of magnitude of large-scale vertical motions in the upper stratosphere, which vary from a few millimeters per second in June, July, and August to a few centimeters per second in December, January, and February.

Webb (ref. 44) has postulated the existence of the "stratospheric tidal jet" following the seasonal reversals at the spring pole. Perhaps more important is the possibility of climatological data bias which the hypothesis introduces. This is because the rocket observations are usually scheduled near noon local time (see fig. 28), and in the summer hemisphere the observations are obtained along the ridge of heated air, and thus sample the minimum temperature gradient and the minimum easterly zonal flow. Higher values of meridional temperature gradient and zonal wind would be expected if the samples were taken in the nighttime sector. Climatological analysis of these data then should provide means which are lower by 10 to 20 meters per second than the actual average easterlies of the summer circulation. In the winter, on the other hand, the rocket observations at noon place the sample in the maximum of the circumpolar westerly circulation. Climatological analyses of those data are then of the maximum in the diurnal variation, and are thus 10 to 20 meters per second stronger than the hemispheric mean. This hypothesis should be investigated to determine the existence of data bias.

SUMMARY AND CONCLUSIONS
Accomplishments

Meteorological Satellites

In 1965 Tiros IX demonstrated that Earth-oriented, global, cloud-cover pictures can be obtained from a spin-stabilized satellite. Thus, development flights required prior to the first flight of the TOS system were completed. (The instrumentation had been previously flight tested aboard Tiros VIII and Nimbus I.) All Tiros spacecraft launched since June 18, 1963, continued to operate in orbit. That is, Tiros VII, VIII, IX, and X were all still capable of providing cloud-cover data as of December 31, 1965. Tiros IX and X were placed into Sun-synchronous, nearly polar orbits similar in objective to that selected for Nimbus I and later for the TOS system.
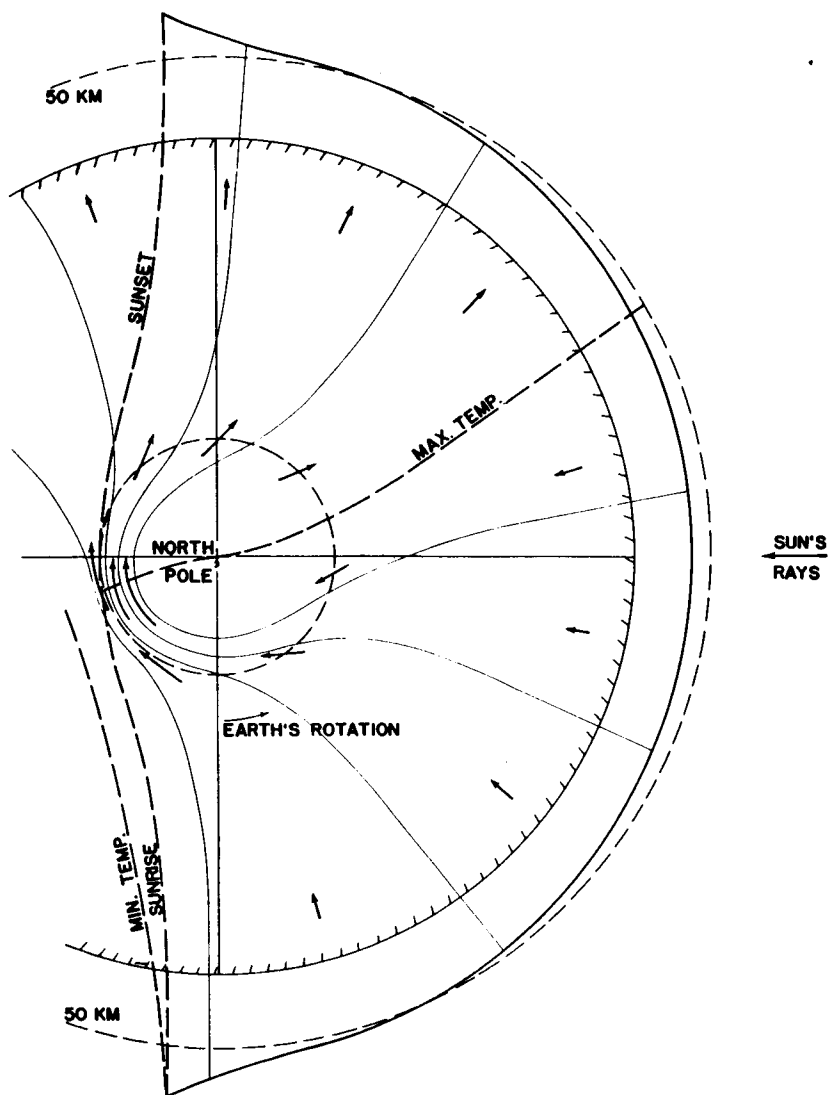
Figure 28.—Equatorial projection of the diurnal stratospheric circulation structure a few weeks after the spring equinox. Diurnal temperature or thickness contours are represented by the thin solid curves and the diurnal circulation is represented by arrows.

The TOS spacecraft (based on Tiros) and the TOS sensors (based on the AVCS and APT developed for Nimbus) have been combined and were completing preflight testing at the end of 1965 for launch early in 1966.

While no further Nimbus spacecraft were launched in 1965, analyses of the spacecraft performance and data continued.

During 1965, an intensive engineering investigation followed which convincingly established the cause of failure and provided a greatly improved design to preclude recurrence of the Nimbus I malfunction. Additional changes have been engineered for the second Nimbus flight to take place in 1966. These changes should significantly improve the performance and increase the value and total yield of scientific data. Perhaps the most notable sensor change will be the inclusion of a multichannel, scanning, medium-resolution infrared radiometer.

The data utilization from Nimbus I operation has provided an estimated average of 70 000 bits of recorded information per orbit despite an eccentric orbit which reduced the observation and transmission times.

Research based on satellite TV cloud-cover pictures continued to produce scientific results in 1965. Some of these are as follows:

(1) Additional criteria were developed for correlating cloud-cover picture data with cyclogenesis or intensification of storm systems.

(2) Indications were found that the classical model of the confluence and difluence of the polar front and subtropical jets with the cirrus clouds on the anticyclonic side of the flow was not always supported by the cloud distribution.

(3) Experiments were conducted to obtain quantitative information on the horizontal field of motion from satellite television pictures and use this information to modify inputs to the numerical analysis in data-sparse areas.

(4) Cloud patterns were related to observed wind speed and direction for both tropical-cyclone and airmass cases.

(5) Cloud and terrestrial albedos were studied using satellite TV picture data.

The radiation measurements provide information on the global distribution of energy sources and sinks and the heat budget of the Earth-atmosphere system. Perhaps the most significant achievement was the completion of 24 months of observing the planet's radiation by Tiros VII. Other achievements include the following:

(1) Medium-resolution satellite radiation measurements have been found useful for the assessment of relative diabatic heating and cooling in the atmosphere on a scale about half the wavelength of the smallest "synoptic" eddies.

(2) Operational applications of meteorological satellite data in-

cluded observation of 40 named tropical storms in 1965. Of these, 5 were hurricanes and 18 were typhoons.

(3) Nonmeteorological applications of the data were particularly evident in cartography, for example, with the 50-mile (80-kilometer) westward movement of the position of Mount Siple on the coast of Antarctica. Geologists have used the AVCS pictures to observe rock, sand, and clay formations on the surface of the Earth. The measurement of sea-surface temperatures by use of IR detectors aboard the satellites was also shown to be feasible.

Meteorological Sounding Rockets

Research meteorological sounding rockets were fired to obtain data up to 100 kilometers at locations from Point Barrow, Alaska, to 60° S (off the west coast of South America) during 1965. Data obtained pertained to the polar winter night, stratospheric warming events, noctilucent clouds, the fine-grain structure of high-altitude winds, and the fall transition period at these altitudes. Analyses conducted during 1965 gave several results.

(1) The magnitude of the total temperature error in measurements taken by the grenade technique was shown to be less than 5 percent.

(2) Further confirmation was found that the absorption of solar radiation by ozone near the 50-kilometer level provides the dominant heat source between the troposphere and the thermosphere.

(3) At the equatorial latitudes, seasonal variations appear to be at a minimum.

(4) The generally accepted circulation patterns cease to exist above about 75 kilometers and the circulation seems to be governed by variations on much smaller time scales than in the stratosphere and lower mesosphere.

The operational development sounding rocket program continued to work toward a low-cost, reliable system suitable for worldwide use. A high-drag, stable-payload parachute has been demonstrated and the rocket-payload environment and aerodynamic characteristics determined during the year.

Scientific results obtained from these operational development-type rockets include the following:

(1) The possible existence of a pronounced semiannual cycle in the zonal wind component at heights of 40 kilometers and above.

(2) Diurnal and semidiurnal oscillations have been noticed with the largest amplitudes near 45 kilometers.

(3) A "stratospheric tidal jet" has been postulated which follows the seasonal reversals at the spring pole and makes known a possible data bias due to the custom of scheduling rocket observations near local noon.

Significant Questions and Outlook

A recent report of a meteorology committee given at the White House Conference on International Cooperation (ref. 45) summarizes the results achieved in meteorology in the past 20 years, and indicates the areas where improvements are required. The advances made in the past 20 years have given scientists confidence that long-range weather predictions of 2 weeks or more ahead will be possible. The largest obstacle at this time is the lack of adequate data for the atmosphere over the entire globe.

The meteorological satellite provides a tool with which to overcome this obstacle. It is a platform with a potential capability of regularly observing and collecting comprehensive atmospheric data over the entire globe. The complete system will include meteorological satellites, horizontal sounding balloons, meteorological ocean buoys, communications satellites, sounding rockets, mathematical procedures for atmospheric models, and high-speed electronic computers.

The role of satellites in the complete system will be multiple. The satellites will observe the atmosphere with their own cameras and sensors and collect data by interrogating horizontal sounding balloons, ocean buoys, and remote land stations. They will communicate these data to processing centers and disseminate weather analyses and forecasts over the world.

Work is progressing to improve the present satellites and their instruments to perform all these functions. Satellite devices for locating and interrogating other platforms are now under development. Instruments are being built to be carried by satellites for sensing the vertical distribution of temperature and humidity of the atmosphere. Cameras and scanners for nighttime observation of cloud cover are being perfected and will be tested soon. Microwave radiometers and spectrometers are under development and are scheduled for tests on future R&D flights. Studies will be made for the overall configuration of future operational satellites to replace the TOS cartwheel configuration presently used.

Sounding-rocket data have been used to further our knowledge and understanding of the atmosphere. Progress is being made in relieving

the scarcity of data by means of both the research sounding rockets
and the smaller operational, development-type sounding rockets.

Eventually it is hoped that the research rockets can be fired from
30 to 50 sites distributed over the world, at an overall rate of several
hundred per year.   During 1965, 43 rockets were fired from 4 sites;
8 more were fired from the U.S.S. *Croatan* which was acting as a
mobile launch platform.   In addition to the research requirements for
data, existence of the capability for obtaining meteorological data
from altitudes up to 100 kilometers has led to requirements for support
to other programs.   These include probes as well as manned and auto-
mated spacecraft.

With both the research and the operational development-type sound-
ing rockets, a major goal is to obtain enough data properly distributed
over the world to allow for the detailed description of the atmosphere
necessary to the much more complete understanding required for reli-
able meteorological predictions up to 100 kilometers.

Many of the significant questions for meteorology will not become
fully known until the observational objectives previously mentioned
have been achieved.   The means of achieving them are the products of
the NASA meteorological programs.

REFERENCES

1. ANON.: Significant Achievements in Satellite Meteorology, 1958–1964. NASA SP–96, 1966.

2. BUTLER, H. I.; AND MOORE, H. S.: The Meteorological Instrumentation of Satellites. NASA, Sept. 1965.

3. RADOS, R. M.; ET AL.: TIROS IX Mission Operations Plan. NASA, Jan. 1965.

4. RADOS, R. M.; ET AL.: TIROS X Mission Operations Plan. NASA, June 1965.

5. NEVILLE, T.: Nimbus Meteorological Satellite Integration and Testing Materials Report No. 8. Document no. 65SD4410, Contracts NAS 5–978 and NAS 5–1347, General Electric Spacecraft Dept., Valley Forge Space Technology Center, Pa., July 1965.

6. PRESS, HARRY: Project Development Plan, Nimbus, Revision 2. Goddard Space Flight Center, Greenbelt, Md., June 16, 1965.

7. HUSTON, WILBUR B.; AND PRESS, HARRY: The Nimbus I Flight. Observations from the Nimbus I Meteorological Satellite. NASA SP–89, 1965, pp. 1–11.

8. ANON.: Nimbus I Post Launch Report No. 2 (Final Report). NASA S–604–64–01, Aug. 27, 1965.

9. ANON.: Nimbus I Users' Catalog: AVCS and APT. Goddard Space Flight Center, Greenbelt, Md., Mar. 1965.

10. Staff of Aeronomy and Meteorology Division: Nimbus I High Resolution Radiation Data Catalog and Users' Manual, Volume 1, Photofacsimile Film Strips. Goddard Space Flight Center, Greenbelt, Md., Jan. 15, 1965.

11. TEPPER, M.; AND JOHNSON, D. S.: Toward Operational Weather Satellite Systems. Astronautics and Aeronautics, June 1965, pp. 16–26.

12. THOMPSON, A. H.; GOSDIN, M. E.; AND JIMENEZ, R. E.: Some Remarks on Cyclogenesis Indications as Determined from Meteorological Satellite Observations, With Application to the Gulf of Mexico Area. Final Report, Grant WBG–17, Dept. of Meteorol., Texas A&M Univ., Aug. 1965.

13. ERICKSON, C. O.; AND FRITZ, S.: Early History of Tropical Storm Katherine, 1963. Monthly Weather Rev., vol. 93, no. 3, Mar. 1965, pp. 145–153.

14. OLIVER, V. J.; ANDERSON, R. K.; AND FERGUSON, E. W.: Some Examples of the Detection of Jet Streams from Tiros Photographs. Monthly Weather Rev., vol. 92, no. 10, Oct. 1964, pp. 441–448.

15. REITER, E. R.; AND WHITNEY, L. F.: Subtropical or Polar Front Jet Stream. Atmospheric Science Technical Paper No. 66, Colorado State Univ., Sept. 1965.

16. HUBERT, L. F.: A Numerical Experiment in Supplementary Tropical Analysis With Satellite Pictures. Geofisica Intern., vol. 4, no. 2, 1964, pp. 85–98.

17. McLAIN, E. P.; RUZECKI, M. A.; AND BRODRICK, H. J.: Experimental Use of Satellite Pictures in Numerical Prediction. Monthly Weather Rev., vol. 93, no. 7, July 1965, pp. 445–452.

18. TIMCHALK, A.; HUBERT, L. F.; AND FRITZ, S.: Wind Speeds From Tiros Pictures of Storms in the Tropics. Report No. 33, Meteorol. Satellite Lab., U.S. Weather Bureau, Feb. 1965.

19. ROGERS, C. W. C.: A Technique for Estimating Low-Level Wind Velocity From Satellite Photographs of Cellular Convection. J. Appl. Meteorol., vol. 4, no. 3, June 1965, pp. 387–393.

20. FRITZ, S.: The Significance of Mountain Lee Waves as Seen From Satellite Pictures. J. Appl. Meteorol., vol. 4, no. 1, Feb. 1965, pp. 31–37.

21. CORBY, G. A.: Preliminary Study of Atmospheric Waves Using Radiosonde Data. Quart. J. Roy. Meteorol. Soc., vol. 83, 1957, pp. 49–60.

22. CONOVER, J. H.: Cloud and Terrestrial Albedo Determinations From Tiros Satellite Pictures. J. Appl. Meteorol., vol. 4, no. 3, June 1965, pp. 378–386.

23. BANDEEN, W. R.; HALEV, M.; AND STRANGE, I.: A Radiation Climatology in the Visible and Infrared From the Tiros Meteorological Satellites. NASA TN D–2534, June 1965.

24. DAVIS, P. A.: Tiros III Radiation Measurements and Some Diabatic Properties of the Atmosphere. Monthly Weather Rev., vol. 93, no. 9, Sept. 1965, pp. 535–545.

25. FOSHEE, L. L.; GOLDBERG, I. L.; AND CATOE, C. E.: The High Resolution Infrared Radiometer (HRIR) Experiment. Observations from the Nimbus I Meteorological Satellite. NASA SP–89, 1965, pp. 13–22.

26. NORDBERG, WILLIAM: Geophysical Observations from Nimbus I. Science, vol. 150, no. 3696, Oct. 29, 1965, pp. 559–572.

27. ALLISON, LEWIS J.; KENNEDY, JAMES S.; AND NICHOLAS, GEORGE W.: Examples of the Meteorological Capability of the Nimbus Satellite. Observations from the Nimbus I Meteorological Satellite. NASA SP–89, 1965, pp. 61–90.

28. WIDGER, WILLIAM K., JR.; BARNES, JAMES C.; MERRITT, EARL S.; AND SMITH, ROBERT B.: Meteorological Interpretation of Nimbus High Resolution Infrared (HRIR) Data, Final Rept. Contract NAS 5–9554, Aracon Geophysics Co., Concord, Mass., Aug. 1965.

29. KUNDE, VIRGIL G.: Theoretical Relationship Between Equivalent Black-body Temperatures and Surface Temperatures Measured by the Nimbus High Resolution Infrared Radiometer. Observations from the Nimbus I Meteorological Satellite. NASA SP–89, 1965, pp. 23–36.

30. NORDBERG, WILLIAM; AND SAMUELSON, R. E.: Terrestrial Features Observed by the High Resolution Infrared Radiometer. Observations from the Nimbus I Meteorological Satellite. NASA SP–89, 1965, pp. 37–46.

31. TAGGART, C. I.; KENNEY, J. R.; AND LEWIS, A. J.: Narrative Account of APT Project NAIREC at Frobisher Bay, Septmeber 1964. Joint Project Report, Meteorological Branch Satellite Data Laboratory (Department of Transport, Canada). National Research Council, Radio and Electrical Engineering Division (Canada), June 1965.

32. TAGGART, C. I.: Interpretation of Geological Features on a Satellite Photograph. Nature, vol. 207, no. 4996, July 31, 1965, pp. 513–514.

33. GROVES, J. R.; WEXLER, R.; AND BOWLEY, C. J.: The Feasibility of Sea Surface Temperature Determination Using Satellite Infrared Data. Final Report, Contract NASw–1157, Aracon Geophysics Co., Concord, Mass., Nov. 1965.

34. Inter-Range Instrumentation Group: Meteorological Working Group, Data Reports of the Meteorological Rocket Network Firings. Document 109–62, vols. XXX to XLII, U.S. Army Electronics Research and Development Activity, White Sands Missile Range, N. Mex., 1964 and 1965.

35. THEON, J. S.; AND NORDBERG, W.: On the Determination of Pressures and Density Profiles From Temperature Profiles in the Atmosphere. NASA TN D–3009, 1965.

36. NORDBERG, W.; KATCHEN, L.; THEON, J.; AND SMITH, W. S.: Rocket Observations of the Structure and Dynamics of the Mesosphere During the Quiet Sun Period. NASA TM–X55251, Apr. 1965.

37. GROVES, G. V.: Meteorological and Atmospheric Structure Studies With Grenades. Space Research: Proceedings of the 4th International Space Science Symposium, Warsaw, June 4–10, 1963, P. Mueller, ed. John Wiley & Sons, Inc., 1964, pp. 155–170.

38. NORDBERG, W.; AND STROUD, W. G.: Seasonal, Latitudinal and Diurnal Variations in the Upper Atmosphere. NASA TN D–703, 1961.

39. WARNECKE, G.; AND NORDBERG, W.: Inferences of Stratospheric and Mesospheric Circulation Systems From Rocket Experiments. Space Research: Proceedings of the 5th International Space Science Symposium. Florence, May 10, 1964, John Wiley & Sons, Inc., 1965.

40. REED, R. J.: The Quasi-Biennial Oscillation of the Atmosphere Between 30 and 50 km Over Ascension Island. J. Atmospheric Sci., vol. 22, no. 3, May 1965, pp. 331–333.

41. ANGELL, J. K.; AND KORSHOVER, J.: A Note on the Variation With Height of the Quasi-Biennial Oscillation. J. Geophys. Res., vol. 70, no. 16, Aug. 15, 1965, pp. 3851–3856.

42. MIERS, B. T.: Wind Oscillations Between 30 and 60 km Over White Sands Missile Range, New Mexico. J. Atmospheric Sci., vol. 22, no. 4, July 1965, pp. 382–387.

43. KAYS, MARVIN; AND CRAIG, RICHARD A.: On the Order of Magnitude of Large-Scale Vertical Motions in the Upper Stratosphere. J. Geophys. Res., vol. 70, no. 18, Sept. 15, 1965, pp. 4453–4461.

44. WEBB, WILLIS L.: Mechanics of Stratospheric Seasonal Reversals. ECOM–5022, U.S. Army Electronics Research and Development Activity, White Sands Missile Range, N. Mex., Nov. 1965.

45. MALONE, THOMAS F.; ET AL.: Report of the Committee on Meteorology of the National Citizens Commission on International Cooperation. The White House Conference on International Cooperation, Nov. 28–Dec. 1, 1965.